3-10-2010

Evaluation of Interplanetary Magnetic Field Tracing Models Using Impulsive SEPs

Brian P. Elliott

EVALUATION OF INTERPLANETARY MAGNETIC FIELD TRACING MODELS USING IMPULSIVE SEPS

THESIS

Brian P. Elliott, 2nd Lt, USAF

AFIT/GAP/ENP/10-M05

DEPARTMENT OF THE AIR FORCE
AIR UNIVERSITY

AIR FORCE INSTITUTE OF TECHNOLOGY

Wright-Patterson Air Force Base, Ohio

The views expressed in this thesis are those of the author and do not reflect the official policy or position of the United States Air Force, Department of Defense, or the United States Government.

AFIT/GAP/ENP/10-M05

EVALUATION OF INTERPLANETARY MAGNETIC FIELD TRACING MODELS USING IMPULSIVE SEPS

THESIS

Presented to the Faculty

Department of Engineering Physics

Graduate School of Engineering and Management

Air Force Institute of Technology

Air University

Air Education and Training Command

in Partial Fulfillment of the Requirements for the

Degree of Master of Science in Applied Physics

Brian P. Elliott, Bachelor of Science

2nd Lt, USAF

March 2010

AFIT/GAP/ENP/10-M05

EVALUATION OF INTERPLANETARY MAGNETIC FIELD TRACING MODELS USING IMPULSIVE SEPS

Brian P. Elliott, Bachelor of Science
2nd Lt, USAF

Approved:

//SIGNED//	
Lt Col Ariel O. Acebal (Chairman)	Date
//SIGNED//	
Lt Col Michael R. Hawks (Member)	Date
//SIGNED//	
Peter J. MacNeice, PhD (Member)	Date

Abstract

Current Interplanetary Magnetic Field (IMF) models are evaluated in this study to determine which model(s) perform an accurate representation of this magnetic structure. These IMF models include the Parker Spiral model, the Potential Field Source Surface (PFSS) model, the Wang-Sheeley-Arge (WSA) model and the ENLIL model. Impulsive Solar Energetic Particles (SEPs) are used as tracers to determine the magnetic structure of the IMF and provide source locations for model comparisons. Each individual model is analyzed, compared to the identified solar source region and a longitude/latitude offset of these traces assigned. The model connection of the PFSS and Parker models is found to provide the lowest latitude and longitude offsets from the identified source regions with RMS values of 21.9 and 18.5 respectfully. Model discrepancies are investigated and suggestions are made to improve model tracing performance.

Acknowledgements

I would first like to express my sincere appreciation to my thesis advisor Lt Col Ariel Acebal, for his guidance and support throughout this thesis effort. His knowledge and enthusiasm in the subject matter made the project exciting, even at times when it seemed like it would drag on forever. He kept me pointed in the right direction even when my mind strayed from the project at hand. Without his guidance this thesis would not have become a reality. I would also like to thank Dr. Peter MacNeice for his extensive knowledge on this subject matter. He patiently answered my questions, which at times were off the wall, and guided me through the details of these models. I would also like to thank each and every member of the NASA Community Coordinated Modeling Center who first got me interested in the project and who made this project possible.

I would like to thank my other committee member Lt Col Michael Hawks for his willingness to read my ramblings and help me mold this document into what it is today. Finally I am grateful for the patience and support from my family who spent many nights reading this document and provided valuable feedback. Without their support this work would not have easily come to realization.

Brian P. Elliott

Table of Contents

Page

Page

List of Figures

Figure Page

List of Tables

EVALUATION OF INTERPLANETARY MAGNETIC FIELD TRACING MODELS USING IMPULSIVE SEPS

I. Introduction

1.1 Background and Motivation

With the dawning of the space age, the near-earth space environment has become populated with commercial, government, and national security assets. Each year, these assets are exposed to a wide host of solar phenomena such as intense x-rays, high density plasmas, and energetic particles. The Department of Defense (DoD) has estimated that disruptions to government satellites from space weather effects cost about $100 million dollars a year [*Lanzerotti et al.*, 2006]. However, space weather has a wider impact than just the near-earth environment. Space weather has also been held responsible for multiple High Frequency (HF) communication blackouts, Global Positioning System (GPS) impacts, and other navigation blackouts. Intense solar storming can therefore have large socioeconomic impacts.

The space environment is characterized by a large presence of energetic particles. Most of the time, these particles are of such low flux that they have little or no impact when they strike the Earth's magnetosphere. However, certain events on the sun can cause the flux of these particles to increase by several orders of magnitude. These events are classified as Solar Energetic Particle (SEP) events and can cause significant impacts when they reach Earth. These impacts include Single Event Upsets (SEUs), increased radiation hazards to astronauts and airline passengers, solar panel degradation, satellite navigation failure, and increased atmospheric drag for low

earth orbiting satellites. With such a wide variety of high cost effects, being able to accurately forecast these particles arrival and intensity becomes important.

While it's still not possible to forecast the precise timing of a solar flare eruption, or even if a flare will produce an acceleration of particles to lead to a Solar Energetic Particle (SEP) event, tracing the magnetic field lines back to the sun will aid in forecasting the likelihood that these events, if they occur, will be directed toward Earth. To perform this trace, an important characteristic of charged particles is noted. In general, these energetic particles are constrained to travel along magnetic field lines that permeate through interplanetary space to reach Earth. In this forecasting scheme, Earth's magnetic footpoint, the magnetic line connecting the Sun to Earth, is mapped to the solar surface. Its proximity to active solar regions can then be used to determine a probability of particles originating from this region to strike Earth. In order to perform the most accurate trace of these field lines, it is first important to understand and characterize the magnetic structure through which these particles travel.

Many models have been developed in the scientific community which can perform such a task. The Community Coordinated Modeling Center (CCMC), a branch of the National Aeronautics and Space Administration (NASA) Space Weather Lab, is a multi-agency partnership that performs research, analysis, and development of next-generation space weather models. This agency is constantly receiving and implementing new space weather models into the operational community; however, these models first need to be verified that they accurately perform the task for which they were developed.

1.2 Project Goals

The goal of this research study is to perform validation and verification studies on a suite of models to determine how well they represent the interplanetary magnetic field by using impulsive solar energetic particles as magnetic tracers. The models to be used in this study include the Wang-Sheeley-Arge model, the Potential Field Source Surface model, and the ENLIL model. The domains of these models vary significantly and require many of these models to be linked. Model performance will be analyzed and trends will be identified. Recommendations of improvements to the models will be provided as well as the physical rationale behind these suggestions. A secondary goal of this project is to determine if the models used in this study improve upon the current DoD solar energetic particle forecasting capabilities.

1.3 Document Structure

Chapter 2 provides a detailed review of the current theories behind SEPs and provides a scientific understanding for the various space weather forecasting models used in this study. Chapter 3 details the methodology by which this research is to be conducted and outlines the selection process used for events in this study. Chapter 4 lists the results of performing these model traces and provides analysis. Chapter 5 summarizes the results, lists final conclusions, and outlines possible future work and model modifications.

II. Background

2.1 Chapter Overview

This chapter is broken into three sections. The first section investigates the mechanics and composition of interplanetary space; in particular, the interplanetary magnetic field through which solar energetic particles travel. The second section deals with the definition and different classes of SEPs. Rationale behind the selection of impulsive SEPs is provided as well as a brief overview of SEP impacts. The last section provides a short background on the various space weather models used in this study. It will provide a physical description of the models, their domains, and their importance to this study.

2.2 The Formation of the Interplanetary Magnetic Field

The sun is a variable star that accounts for approximately 99.86% of the mass in the solar system. It is composed primarily (98%) of hydrogen and helium and about 2% of other elements. All these elements exist in a gaseous plasma state to form layers within the sun. The innermost layer is the core of the sun. This layer is very hot (approximately 14 million Kelvin) and is responsible for the conversion of hydrogen to helium; releasing energy in the form of nuclear fusion. The second layer of the sun is the radiative zone, so named for the process through which this layer transports energy. The temperature of the plasma in this layer decreases from the values in the core and nuclear fusion is no longer able to be sustained. Combined with the core, these two layers comprise approximately three-fourths of the sun's radius. Enveloping this radiative zone is the convection zone. Again the temperature decreases in this layer and the primary method of energy transfer is convection. It is within this layer that the sun is believed to form its basic magnetic structure due

to the differential rotation of this layer with the outer layers. The details on the formation of this magnetic field are not well understood and the interested reader is referred to [*Foukal*, 2004] for further theory on the creation of this magnetic field. At the outer boundary of the convection layer lays the photosphere; the visible surface of the sun. Photospheric plasma is relatively cool (approximately 6000 Kelvin) and it is on this surface that satellites and ground-based observatories image sunspots and other solar features. By observing these solar features and how they move across the surface of the sun, it becomes possible to determine the sun's rotation rate.

Richard Carrington in 1850 determined this rotation rate to be 25.38 days by observing the motion of sun spots. This rate is the sidereal rotation of the sun; the time it takes the sun to rotate one full revolution relative to the stars. However, the Earth rotates in the same direction as the sun; therefore the solar rotation time would be slightly longer than the sidereal rotation period with respect to an observer on Earth. This new rotation period, called the Carrington rotation, is 27.3 days. This is the time it takes for the sun to complete one revolution as observed from Earth. Scientists have been keeping track of the number of times the sun has rotated starting with Carrington rotation (CR) 1 in 1853. At the beginning of the year 2010 the Carrington rotation number was 2092.

Scientists identify the location of sunspots with regard to the location of the sub-Earth point, such as N17 W65. This number indicates that the spot in question was located 17° north of the equator and 65° west of the central meridian as viewed from Earth. It was therefore important to consider that the sun rotates underneath the Earth as it progresses through its rotation. The next day (after the initial observation of the sunspot) all features on the sun, assuming they are static on the surface, have progressed $\frac{360^\circ}{27.3 \text{ days}} = 13.19^\circ$. When examining past events it becomes necessary to take into account the heliographic longitude and latitude of the sun. The heliographic

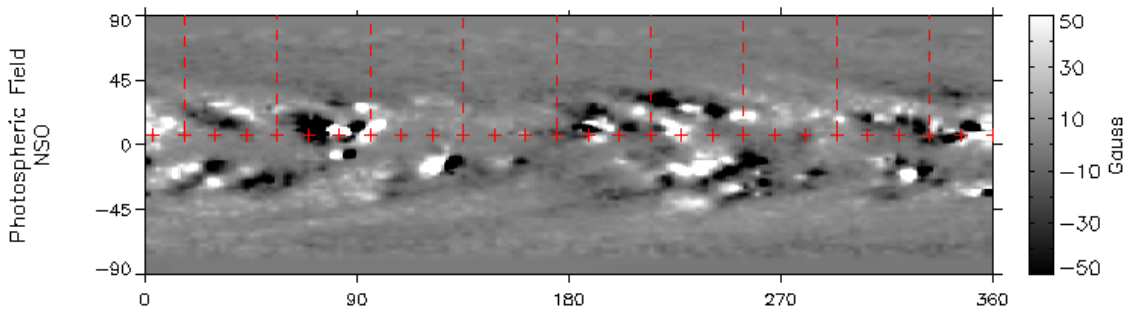

Figure 1. A Sample Magnetogram from Carrington Rotation 1967

(or Carrington) longitude (L_0) takes the solar rotation into account. This value starts at 360° when a new Carrington rotation begins and decreases to a value of 0° as this period nears its end. The heliographic latitude (B_0 not to be confused with magnetic field strength) takes into account the suns tilt to the ecliptic plane and varies from ±7.23°. These parameters will become necessary in order to compare coordinates obtained by running the models with the coordinates of the confirmed source locations given by various authors used in this study.

Each day several solar observatories take several images of the sun. These images are used to measure solar features, such as sunspots, to help determine the state of the sun. Amongst these images taken is a magnetogram, a pictorial representation of the magnetic strength and structure of the sun. These images are taken from a Michelson Doppler Imager (MDI) which determines this magnetic structure using the Zeeman Effect. By combining these individual magnetograms over a solar rotation, a synoptic magnetogram is formed (figure 1). This synoptic magnetogram was used as input to many of the models in this study.

The outer layers of the sun are considered part of the sun's atmosphere. The first of these layers is the chromosphere. Within this layer, the temperature of the plasma rises slightly from the photosphere and the density decreases. At the outer boundary of the chromosphere is a very small region known as the transition region. It is within

this region that the temperature of the plasma rises significantly (to approximately two million Kelvin). The last layer of the sun, called the corona, extends out into interplanetary space. The temperature of the plasma within this region continues to increase. Due to the large amount of thermal energy these particles are accelerated to, a fraction of them are able to escape into space forming what is called the solar wind.

The solar wind is an ever present feature of the sun composed of the very tenuous plasma ejected from the solar corona. As this plasma leaves the sun, it flows radially outward in all directions and drags the solar magnetic field with it into interplanetary space. The interaction of the magnetic field with this plasma is responsible for the magnetic structure present in interplanetary space.

The behavior of plasma in the presence of magnetic field can be described by the magnetohydrodynamic (MHD) magnetic induction equation. The derivation of this equation is a straightforward manipulation of Maxwell's equations and can be found in appendix A. This equation, listed below, contains three terms: the term on the left is the time rate of change of the magnetic field; the first term on the right hand side, containing the velocity of the fluid, $\vec{u}$, is called the convection term; and the last term, which contains the conductivity of the plasma, σ, is called the diffusion term. For a time-dependent magnetic field, one of the terms on the right side will typically dominate.

$$\frac{\partial \vec{B}}{\partial t} = \vec{\nabla} \times (\vec{u} \times \vec{B}) + \frac{1}{\mu_0 \epsilon_0} \nabla^2 \vec{B} \tag{1}$$

A dimensionless parameter used in determining which of these terms dominates is called the magnetic Reynolds number. This number shows the ratio between the convection and diffusion terms

$$R_m = \frac{|\vec{\nabla} \times (\vec{u} \times \vec{B})|}{|\frac{1}{\mu_0 \sigma} \nabla^2 \vec{B}|}. \tag{2}$$

If $R_m << 1$, then the diffusion term dominates and the magnetic field can diffuse through the plasma. In this case, the magnetic field is not heavily influenced by the motion of the plasma. On the other hand, if $R_m >> 1$, then the convection term dominates and the magnetic field is linked with the motion of the plasma [*Gurnett and Bhattacharjee*, 2005]. The plasma present in the solar wind is characterized by a very high conductivity $\sigma >> 0$ and therefore a high magnetic Reynolds number. The condition when $R_m >> 1$ is known as the frozen flux theorem and the magnetic fields behave as if they move with the motion of the plasma.

With this knowledge, the formation of the IMF can be explained (figure 2). To determine if solar plasma is released from the sun, it it important to understand the balance of gas kinetic pressure and magnetic pressure. The gas kinetic pressure is the pressure exerted per unit area by the kinetic energy of the gas particles. The magnetic pressure is identical to any other physical pressure, much like the kinetic energy of the particles when considering gas pressure, except this pressure is carried by the magnetic field. Since the background magnetic field strength of the sun is relatively weak the gas pressure usually dominates and solar plasma is released into space. Under certain conditions, however, the local magnetic field strength can exceed the gas pressure and in this case, the plasma is restrained by the strength of the magnetic field. Assuming the gas pressure dominates, as solar material is ejected in the form of the solar wind, it is released radially outward. If the magnetic field is frozen into the plasma, the solar wind drags the magnetic field out with it. After a finite amount of time the sun has rotated and the source region that released the particles has moved toward the west. However, the plasma parcel released at the first time step is still following a radial field line from the source region on the sun. After several

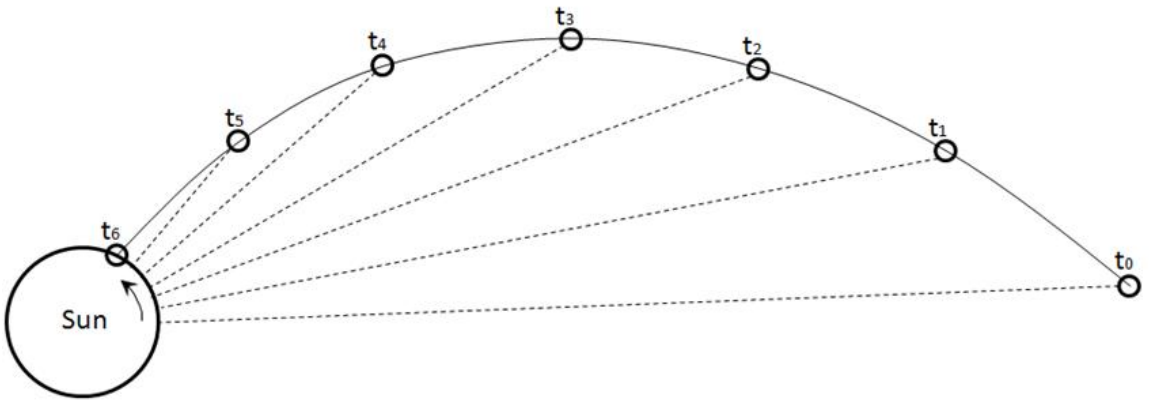

Figure 2. The Formation of the Archimedean Spiral Shape of the IMF

time steps an Archimedean spiral shape takes form. This is analogous to a rotating garden sprinkler. The water travels radially outward from the nozzle of the sprinkler, analogous to the solar wind emanating radially away from the sun. As time progresses an Archimedean spiral shape takes form, analogous to the basic magnetic structure of the IMF (figure 3).

The only way to change the shape of this spiral would be to alter either the rotation of the sun or the speed at which these particles are released. Since the rotation of the sun is fairly constant, this leaves only the solar wind speed to alter this basic structure. For a fast solar wind the particles can travel much farther in a given constant time step. As this speed approaches infinity, the field lines approach straight radial lines from the source region. At infinite solar wind speeds, the sun does not have time to rotate beneath these plasma parcels. In contrast with the same time step, a slower solar wind will result in more wrapping of this spiral as the time it takes the parcel to reach a given location, the sun, will have had time to rotate several degrees. Figure 3 shows the Archimedean spiral shape of the IMF using two separate solar wind speeds. The yellow line indicates the shape if the solar wind were accelerated to $2000\,km\,s^{-1}$ while the red line shows the structure of the IMF using an average solar wind speed of $400\,km\,s^{-1}$.

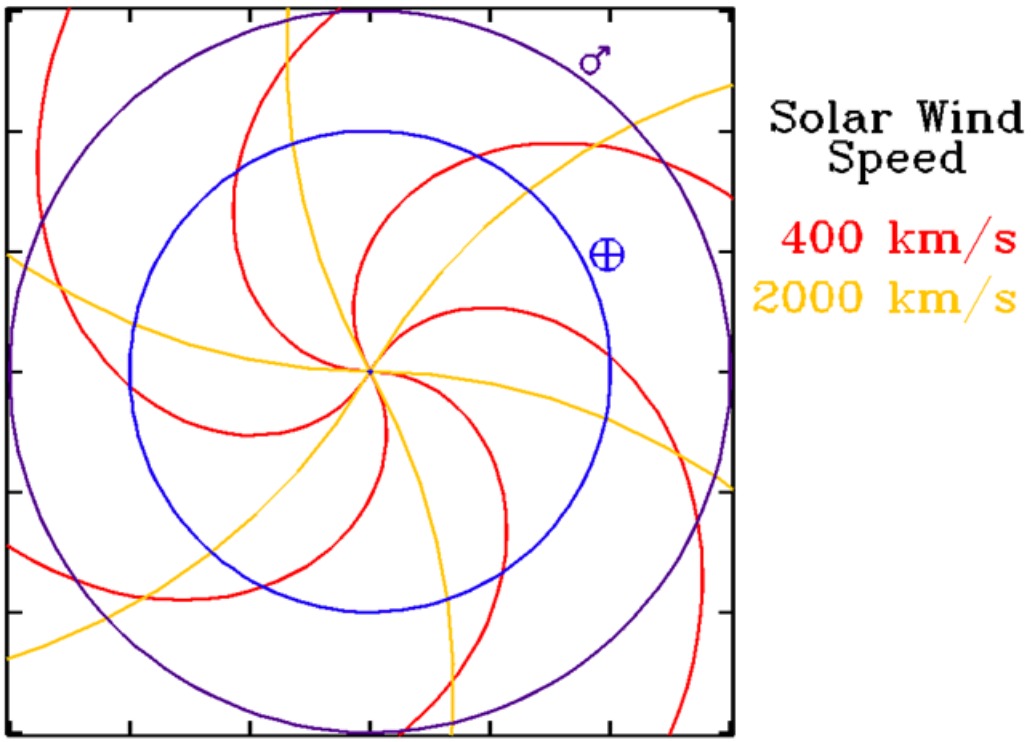

Figure 3. IMF Structure Showing Solar Wind Dependence

This Archimedean spiral is a simple model for the structure of the IMF. However, in reality the IMF has more structure to it. One of the features which adds to this structure is the heliospheric current sheet. The sun's main magnetic field is much like a magnetic dipole. Thus as field lines are pulled out into space they have associated with them a magnetic polarity. Physics alludes to the nonexistence of magnetic monopoles $\nabla \cdot \vec{B} = 0$. Thus as the magnetic field lines of one polarity are stretched outward into the IMF by the solar wind, the same line must reconnect back to the sun on an opposite polarity field line. This reconnection is theorized to take place near the heliopause of the solar system located at ≈ 100 Astronomical Units (AU's) or 100 times the distance from the Earth to the Sun [*Prölss*, 2004]. As field lines from the northern hemisphere approach the equatorial plane of the sun (figure 5) they come in close proximity to field lines of opposite polarity originating from the southern hemisphere. The local current density is related to the spatial derivative of field strength. In the thin region where these field lines of opposite polarity approach close to one another, these derivatives become large, implying the existence of strong current density (figure 4). This thin region is know as the heliospheric current sheet. This magnetic feature adds complexity to the basic structure of the IMF (described above) as particles which are constrained to follow a particular magnetic field line cannot, in general, cross this sheet.

The Earth is located near this ecliptic plane of the sun (figure 5); however, the sun's orbit has an inclination of 7.25°. Therefore, as the sun completes one solar rotation about its axis, the Earth will be located above and below this current sheet. At one point during a solar rotation, observations at Earth will indicate a radial component of the B field pointing toward the sun; while, at a different time during the same solar rotation, this field will be directed away. In addition, this current sheet does not always occur precisely in the equatorial plane. Often times, these oppositely

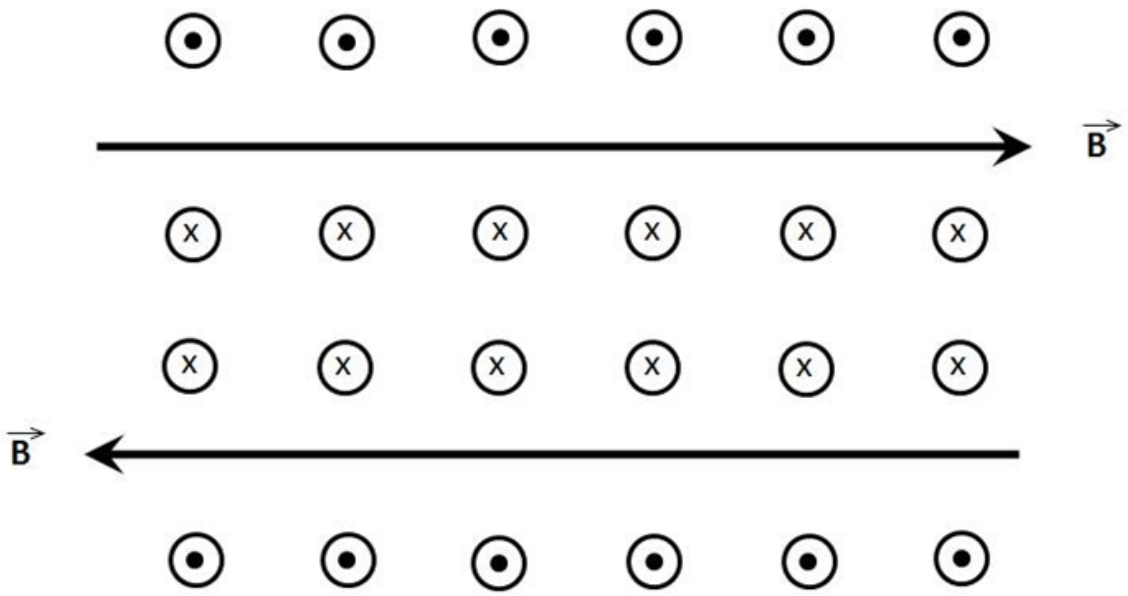

Figure 4. The Formation of the Heliospheric Current Sheet

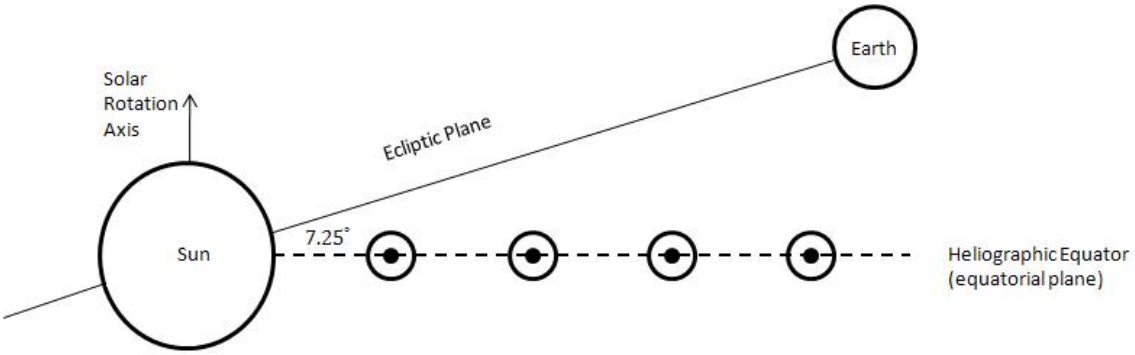

Figure 5. The Orbit of Earth with respect to the Sun's Equatorial Plane Demonstrating the Variability in the Current Sheet

directed field lines will move about the equatorial plane adding to the amplitudes of the oscillations.

Due to the dependence of the IMF structure on the solar wind, it should come as no surprise that any change in the solar wind speed affects the predictions of this spiral model. Faster solar winds will form a smaller angle with Earth as these particles do not have as much time to form into a spiral as their slower counterparts. This fast solar wind originates from coronal holes, a solar feature which rotates with the sun. A coronal hole is a region in the corona where cooler, low-density plasma is associated with open magnetic field lines protruding out into interplanetary space [*Foukal*, 2004]. An open magnetic field is defined to be a magnetic line emerging from one region that does not return to a conjugate region but rather extends into interplanetary space. These high speed streams can interact with the slower solar wind ahead of it and introduce co-rotating interaction regions within the IMF, a feature that adds to the complexity of these magnetic traces.

The sun is variable and approximately every eleven years completes a solar cycle. This period is based on the swapping of the sun's magnetic poles. At the beginning of the cycle, the surface magnetic configuration is relatively simple and resembles that of a magnetic dipole. As the solar cycle progresses, these field lines become twisted and contorted due to the differential rotation rates of the photosphere and the convective zone. The surface field lines grow in complexity with the appearance of active regions and sunspots containing strong localized magnetic fields. This period of increased magnetic complexity is referred to as solar maximum. Figure 6 shows the variability of the sun over a ten year period. The bright spots indicate active regions where these contorted magnetic fields have pushed through to the surface. In 1996 and 2006, the sun was at solar minimum and very little activity was observed, evident by the lack of these active regions on the solar surface. In contrast, 2001 marked the year of solar

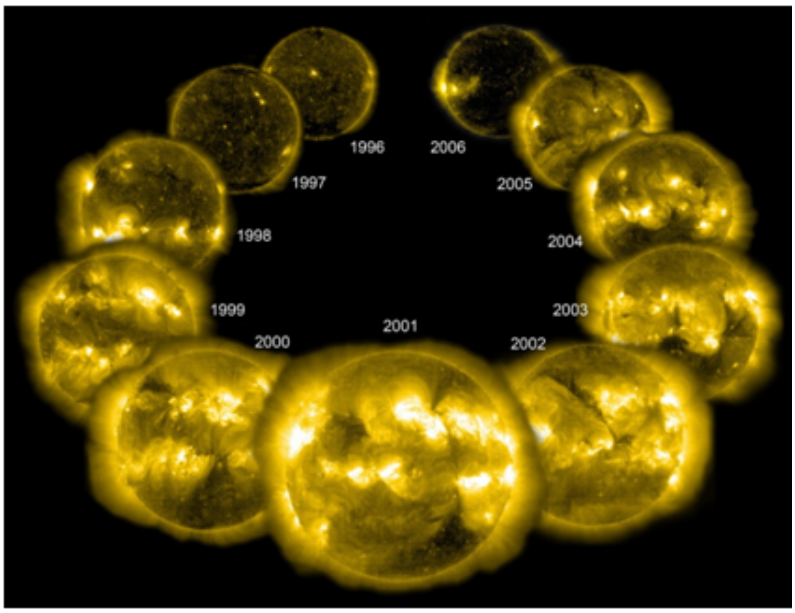

Figure 6. Depicts the Progression of the Solar Cycle. Image courtesy of SOHO/EIT consortium. SOHO is a project of international cooperation between ESA and NASA

maximum where these active regions covered a large portion of the sun.

When active region magnetic fields become to stressed they can relax explosively. Magnetic reconnection occurs relieving stress in the field and in the process converting magnetic energy into other forms including the kinetic energy of Coronal Mass Ejections (CMEs), hot plasma which radiates in white light, Extreme Ultraviolet and X-rays, solar flares, and in the form of accelerated energetic particles. Solar flares are caused by a rapid energy release in the solar corona, believed to be driven by stored, non-potential magnetic energy and triggered by an instability in the magnetic configuration [*Aschwanden*, 2004]. A CME is generated when an intense magnetic explosion occurs on or near the surface of the sun. These explosions eject contorted magnetic flux tubes along with solar plasma into space. These two solar features cause an acceleration of nearby plasma particles to high energies and these particles sometimes escape into space where they can impact Earth. Particles accelerated in this fashion are called Solar Energetic Particles (SEPs).

The frozen flux theorem states that plasma parcels linked together by a magnetic field line will always remain on the same field line (diffusion term is zero). Charged particles will, therefore, remain associated with a specific field line as they propagate through the IMF. It is this physical relationship between the plasma and magnetic field that allows the tracing of SEPs to be performed. However, an important assumption was made in this analysis. Although the conductivity of the solar wind is high, it is not infinite and therefore an assumption must be made that the contribution from the diffusion term is significantly small and can be neglected. In general, this is true for the solar wind; however, the diffusion term is not altogether zero. This fact allows some charged particles to scatter across magnetic field lines within the IMF.

2.3 Different Classes of SEPs

The first evidence of high-energy particles from the Sun were obtained in 1946 when Forbush used sea-level ion chambers to mark differences in cosmic ray intensities during the solar events of early 1942. Forbush noticed that an increase in these intensities were preceded by radio blackouts and bright chromospheric eruptions or solar flares [*Forbush*, 1946]. He theorized that a possible source of acceleration for these energetic particles could originate from the observed solar flares. This was the first theory that incorporated energetic particles originating from the sun. As science grew and better equipment was built to monitor both the sun and energetic particles, Forbush's theory was proven correct.

Since the beginning of the space age, satellites have provided in situ measurements of the space environment. Much research has gone into determining the origins and acceleration of these particles, and from this, two different classes of SEPs have been identified. These classes include impulsive and gradual SEPs in reference to the timescale of the accompanying soft X-ray flux [*Reames et al.*, 1994]. Up until the early

70's, it was thought that all energetic particles arriving from the sun were accelerated locally from flare sites. However, a strong CME, erupting on December 14, 1971, over the southeast limb of the sun, was the first hint that SEPs may have more than one acceleration mechanism [*Kahler*, 2001]. This CME event led to a sudden onset of SEPs near Earth which for that particular event could not be explained by the flare acceleration method. An investigation followed and a new acceleration mechanism was found.

This new acceleration method for creating gradual SEPs is thought to occur by shock waves being driven out from the sun by fast moving CMEs. The magnetic cloud released by the CME is ejected faster than the background solar wind and thus forms a shock front ahead of it where the acceleration of these SEPs are thought to occur. For a detailed overview of CME particle acceleration and ejection, please see [*Moore and Sterling*, 2006] and [*Klimchuk*, 2001]. Since the acceleration takes place at the shock front, energetic particles are no longer constrained to follow the magnetic field lines from the sun where the event originated, making it somewhat harder to determine their solar source locations.

Gradual SEP events typically have long onset times and last much longer than impulsive events, on the order of days. These events are usually proton-rich, have low Fe/O elemental ratios, and are associated with type II solar radio bursts [*Tylka et al.*, 2005b]. Due to the nature of this acceleration method, particles can be accelerated along the shock front which often spans many degrees. Therefore, the particles observed at Earth accelerated from this shock front could have originated anywhere along that front and no precise location is available to compare the model traces to. In addition, CMEs distort the IMF as they propagate through; further adding complexity in the IMF. For reasons mentioned, these types of events will not be used as magnetic traces for this study.

The other class of SEPs, and the one considered for use in this study as magnetic tracers of the IMF, are called impulsive SEPs. According to *Reames* [1995] these events are usually electron rich with higher Fe/O elemental ratios than the gradual events. The particles in these events are believed to be accelerated in the solar flare itself, giving rise to a sudden onset of these particles. Due to the nature of the acceleration method, these events typically last only hours and are usually associated with type III solar radio bursts.

The energy released during a solar flare is enough to accelerate a small fraction of the nearby solar plasma to high energies and these particles, when they escape into space, are the source of the impulsive SEPs. Solar flares typically occur in the presence of an active region. These active regions contain twisted, closed magnetic field lines. However, in order for these particles to escape into space, they must travel along open magnetic field lines. Therefore, the particles released from a solar flare must scatter to a nearby open magnetic field line in order to propagate into space.

These open field lines connect the particles to the IMF where they join the solar wind and propagate outward. With an identifiable likely acceleration source region on the sun and the fact that these particles are assumed to be constrained to follow these magnetic field lines, these particles serve as magnetic tracers of field lines within the IMF, allowing the model traces to be compared to the solar flare location.

One way to help distinguish between these two particle acceleration mechanisms are solar radio bursts. These bursts are caused primarily by the acceleration of electrons. Due to the non-collisional processes that create these bursts, radio waves are often used to probe the acceleration of these electrons in different solar regions. This leads to a variety of different types of bursts. The ones of primary importance when studying SEPs are the type II and type III radio bursts. Type II radio bursts cover the 20-150 MHz frequency range, typically last 3 to 30 minutes, and are thought

to be produced by electron acceleration at MHD shock fronts by complex plasma processes [*Gopalswamy*, 2006]. These types of emissions are attributed to slow drift electrons and are thus typically associated with gradual type SEPs.

In contrast, type III solar radio bursts are on the order of 100 MHz and have much higher drift rates. These emissions are thought to be caused by a stream of electrons following magnetic field lines. These last only a few seconds to several minutes and are typically associated with solar flares and impulsive SEP events [*Cliver and Ling*, 2009].

2.4 Space Weather Models

Performing a magnetic trace using a suite of space weather models currently held at the CCMC is the primary focus of this study. This section deals with describing the physics behind these models, their domains, and the importance to this study. The models used to perform this trace of impulsive SEPs are the Potential Field Source Surface model (PFSS), the Wang-Sheeley-Arge model (WSA) sometimes referred to as the Arge model, the ENLIL model, and a simple Parker spiral.

2.4.1 The Parker Spiral Model.

The Parker spiral model requires the least amount of input data and is the simplest out of the models used in this study. This model is based on the Archimedean spiral shape of the magnetic field lines as described earlier in this chapter. As this solar plasma moves radially outward from the sun, it drags the magnetic field lines with it. As this plasma continues to move radially outward, the sun has rotated and this rotation now gives the field line a curve. As more time passes the field line continues to become stretched into a spiral shape due to the constant rotation of the sun.

At Earth, the field lines hit with a certain angle, usually described as χ. This

angle depends on how much the sun has moved in the time that it takes the plasma to reach Earth. The plasma carrying this magnetic field is traveling with the solar wind velocity and therefore knowing the solar wind speed is necessary in order to perform this calculation. The solar rotation rate will also be required as this will determine how far the sun has moved in the time it takes the plasma to reach Earth.

The sun is made up of highly ionized plasma and has a differential rotation rate depending on latitude. The rate of rotation is observed to be faster at the equator and fall off as one approaches the poles. Earth is located very near the equatorial plane of the sun and only varies by $\approx \pm 7$ degrees. Therefore an assumption that the Earth is located on the solar ecliptic ($\lambda = 0$) is made in order to make the calculations easier. Now a solar rotation rate can be determined based on the rotation speed of the solar plasma near the equator.

One last thing remains to be described before a final form of the modified Parker model can be determined. This model will be linked to the PFSS model whose outer boundary is located at 2.5 $R_{\odot}$. Therefore, it is necessary to determine how much the field line is shifted at this radial boundary. After combining all the above information, the final Parker model equation, modified for the specific purpose of use in this study, can be defined by the following equation:

$$\phi_E = \Omega_{\text{carr}} \left(\frac{r_E - R_{ss}}{\nu_{sw}} \right) + \phi_{\text{CM}}. \tag{3}$$

ϕ_E is the longitude of the field line which intersects the solar surface, r_E is the distance from sun to Earth (1 AU), R_{ss} is the source surface for the particular model in question, Ω_{carr} is the Carrington rotation rate described above, ν_{sw} is the solar wind speed, and ϕ_{CM} is the heliographic longitude at the time of the event.

It is important to note some of the assumptions made when deriving this equation. First off, the solar wind speed is assumed to be constant from its source location near

the sun all the way to Earth. This is in fact not true, as the solar wind begins subsonic and accelerates as it makes its journey outward. By neglecting this the model will trace to a source location farther toward the west limb than is likely the case. Another assumption is the negligence of the zonal component of the solar wind. It is assumed that the solar wind was created from the plasma that streams outward from the sun; however, this plasma rotates with the sun at a certain velocity before it decouples and travels outward. According to Prölss this zonal component of the solar wind is small $\approx 6\,km\,s^{-1}$. This can be safely ignored in this particular case as the distance in which the solar wind plasma becomes decoupled is small in comparison to the distance from the sun to Earth.

This model is currently used by DoD as a part of the SEP arrival forecast. This is accomplished by examining active regions on the Sun, determining how close these regions are to the field line that is connecting Earth to the Sun. Although its still not possible to forecast the precise timing of a solar flare or even if the flare will accelerate particles, if an active region is close to the Earth connection region and flares do occur, a probability can be determined to evaluate the possibility of these particles reaching Earth. Perhaps the biggest problem with this current forecasting scheme is the inability to take into account the latitude of the active region that may accelerate these events. If the Earth is located on one side of the current sheet but the flaring region occurs on the opposite side of the current sheet, the particles would not be expected to traverse through this current sheet; however, the Parker model has no capability of tracing the latitude of the these field lines and therefore would not account for this feature.

2.4.2 The Potential Field Source Surface Model.

The PFSS provides an approximate description of the solar coronal magnetic field based on observed magnetograms as input. The model solves Laplace's equation within an annular volume above the photosphere in terms of a spherical harmonic expansion, the coefficients of which are calculated by the Wilcox Solar Observatory. Coronal currents are neglected so as to allow unique solutions in closed form. To circumvent the problem that such simple harmonic expansions would result in all of the magnetic field lines returning to the sun, an outer radial boundary is established by which point the coronal field is required to become radial [*Riley et al.*, 2006]. It calculates these magnetic fields from the surface of the sun, assumed to be one solar radius, out to a source surface which is set by the user. The range of acceptable values is 1.6-3.25 solar radii with 2.5 the default and recommended value. In this study, this model will be linked with a normal Parker spiral to determine the footpoint of the magnetic field line connecting Earth to the sun. *Schatten et al.* [1969] provides a detailed description of this model.

2.4.3 The Wang-Sheeley-Arge Model.

The WSA model has two components: the inner WSA Potential Field and Current Sheet model (WSA PF+CS); and the outer WSA Inner Heliosphere Model (WSA-IH). The WSA PF+CS model serves as the inner coronal component of the complete WSA model to combine a pfss model, similar to the one described in the last section, with a current sheet model to produce a model of the global coronal magnetic field between the solar surface and a bounding spherical surface (R_{cs}) typically set at $5R_{\odot}$. Much like the PFSS, this inner model assumes the magnetic fields to be radial at this boundary and determines the magnetic polarity of the field lines from synoptic magnetograms. In this study, this magnetogram data is provided from either the

Kitt Peak or Mount Wilson solar observatories. At this $5R_{\odot}$ boundary, the model calculates the solar wind speed using an empirical relationship based on the divergence of the magnetic field and the proximity of the selected open field line footpoints to the nearest coronal hole boundaries. The outer WSA-IH model uses simple kinematic processes to propagate the solar wind and the magnetic polarity, from this outer boundary, into the heliosphere out to a distance of 1 AU. In this study, however, the model is linked with the ENLIL heliosphere model to propagate the field lines to Earth. This connection of models requires an extension to be made to the R_{cs} surface. Instead of this boundary occurring at $5R_{\odot}$, this surface is extended to $21.5R_{\odot}$. Throughout the remainder of this document, the investigation will only be concerned with the WSA as it is linked to the ENLIL model. Therefore, the WSA is considered a whole model whose domain ranges from the solar surface to the boundary of $21.5R_{\odot}$ which will be refereed to as R_{cs}, where this model is then connected with the ENLIL model. *Arge and Pizzo* [2000] provides a detailed description of this model.

2.4.4 The ENLIL Model.

ENLIL (named after the Sumerian god of wind) is a time-dependent 3-dimensional magnetohydrodynamic model of the heliosphere. It solves equations for plasma mass, momentum, energy density, and magnetic field. Its inner radial boundary is located beyond the solar wind sonic point, typically at 21.5 or 30 solar radii. The input to this model comes from the WSA output described above. The output from the WSA model provides the starting plasma parameters for the ENLIL model. The outer radial boundary of this model can be adjusted to maximum value of 10 AU although for the purpose of this study a range of 1.5 AU is sufficient. It covers 60 degrees north to 60 degrees south in latitude and 360 degrees in azimuth. This model is linked with the WSA and is responsible for tracing the magnetic field lines between the WSA

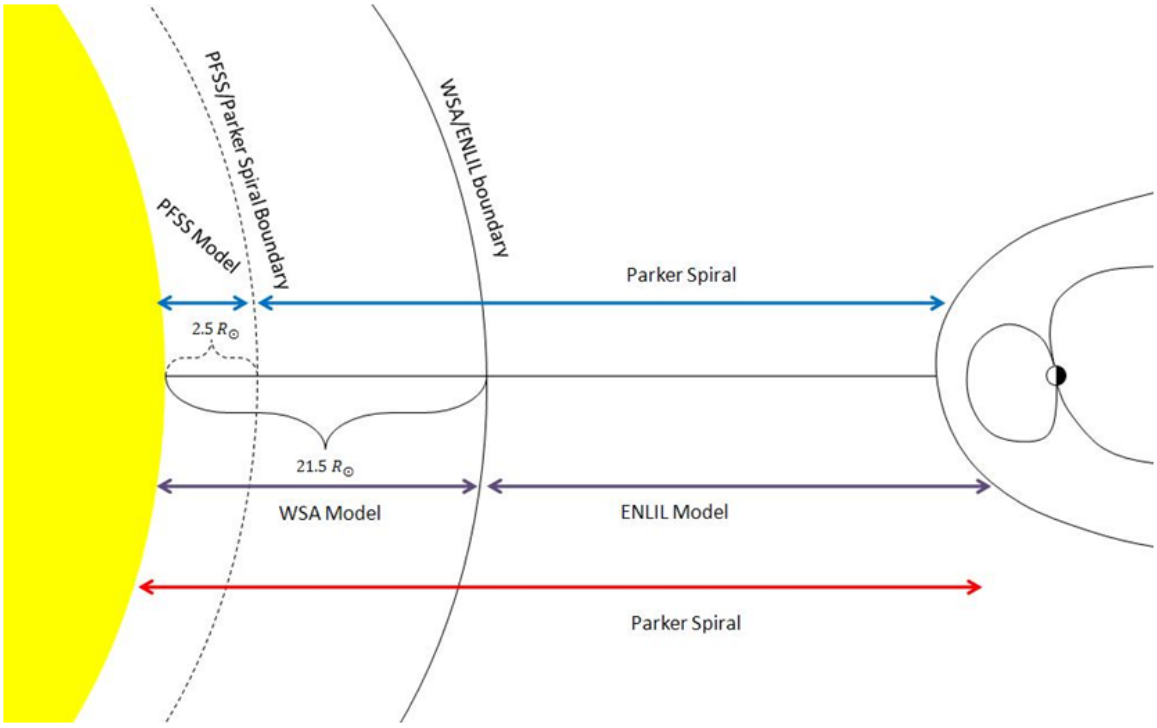

Figure 7. Domains of the Space Weather Models Used in this Study

$21.5R_\odot$ surface and Earth. Figure 7 depicts the various model linkages discussed thus far as well as their domains.

III. Procedures

3.1 Chapter Overview

This chapter describes the procedures used to perform this study. It is broken into three sections. The first deals with the selection of the magnetic tracer events used for validation of the models. The criteria used to select the various events is reviewed and a final list of events is provided. The second section deals with the different model runs. This section provides details on how the various models used in this study are run and how the models input data was obtained. The last section describes the metrics used to compare these models.

3.2 Magnetic Tracer Event Selection

In order to begin tracing the various models, it was necessary to select SEP events which had identified source regions on the surface of the sun. As discussed earlier, only impulsive SEP events were used due to the relatively simplistic IMF they provide. Many researchers have made their own lists of SEPs and identified their likely source region on the surface of the sun. The first step was to search through the current literature to locate articles that provide such a list. Table 1 outlines the articles selected for their lists of SEPs.

Table 1. Articles Listing SEP's

Author	Title	Publication Year
Cane et al.[1]	Two Classes of Solar Energetic Particle Events Associated with Impulsive and Long Duration Soft X-ray Flares	1986
Cohen et al.[2]	New Observations of Heavy-Ion-Rich Solar Particle Events from ACE	1999
Desai et al.	Heavy-Ion Elemental Abundances in Large Solar Energetic Particle Events and their Implication for the Seed Population	2006
ESA	List of Solar Energetic Particle Events	2009
Kurt et al.	Statistical Analysis of Solar Proton Events	2004
Laurenza et al.	A Technique for Short-Term Warning of Solar Energetic Particle Events Based on Flare Location, Flare Size, and Evidence of Particle Escape	2009
Nitta et al.[1]	Solar Sources of Impulsive Solar Energetic Particle Events and their Magnetic Connection to the Earth	2006
Reames and Ng[2]	Heavy-Element Abundances in Solar Energetic Particle Events	2004
SWPC	Solar Proton Events Affecting the Earth Environment	2009
Tylka et al.[1]	Shock Geometry, Seed Populations, and the Origin of Variable Elemental Composition at High Energies in Large Gradual Solar Particle Events	2005
Wang et al.[1]	Coronal Holes, Jets, and the Origin of ^{3}He Rich Particle Events	2006
Yashiro et al.[1]	Association of Coronal Mass Ejections and Type II Radio Bursts with Impulsive Solar Energetic Particle Events	2004

[1] Author classified SEP event and provided source location
[2] Author classified SEP event

By compiling all data from these lists a total of 1153 separate SEP events occurred on different days spanning from 1970-2007. Out of the twelve articles selected, only seven classified the event as impulsive or gradual (see footnotes of table 1). Events classified as gradual were not included, leaving a list of the remaining impulsive identified SEP events. Also events that were simply classified as mixed or unknown were thrown out to avoid uncertainties in the IMF. This narrowed the list down to 88

impulsive events ranging from 1979-2003. Out of the seven articles that classified the events as impulsive, only five provided a possible source region for these events (see footnotes of table 1). When a trace of these particles was performed, the results were compared to an identified acceleration source region; therefore all events selected must contain an associated identified source acceleration region. In an effort to mitigate the selection error for these events, a requirement that at least two separate authors from the five articles classified the event as impulsive as well as give a likely acceleration region for these particles was imposed. This narrowed the list down to 25 possible events. Another restriction was then imposed in which all data from 24 hours prior to the selected SEP event was scanned to determine if another impulsive or gradual SEP event was recorded. The data, used to determine if another SEP event occurred, was taken from the master list compiled at the beginning of this study. This eliminated five of these events; leaving a total of twenty events (table 2) from three separate authors upon which this study was to be performed.

With the selection of the tracer events completed, it was important to note the different classification schemes used by the various authors in determining when an impulsive event occurred. The following paragraphs describe each authors classification scheme before the individual events were screened and selected. This was performed in order to help in later analysis of the models to determine any potential sources of error.

Yashiro selected a total of 38 impulsive events between January 1996 and April 2002 by investigating data from the EPACT instrument on board the WIND spacecraft in the 2-3 MeV amu^{-1} region. In order to classify the event as impulsive, Yashiro demanded the event either contains particles with ^{3}He/^{4}He > 1 or those with Fe/O > 1 and ^{3}He/^{4}He > 0.1. In addition, these events were required to show clear onsets with velocity dispersion (earliest arrival of the particles with highest energy) and to

have a He intensity exceeding 10^{-3} (cm^{2}sr s MeV/amu)$^{-1}$. In order to identify the source region of these events, Yashiro used the associated interplanetary type III radio bursts observed by the WAVES instrument on board the WIND spacecraft [*Yashiro et al.*, 2004].

Table 2. List of Events Used for Study

SEP Event Number	SEP Onset Date and Time	Carrington Rotation Number	Identified Source Location		
			Nitta	Yashiro	Wang
1	Sep 17 1997 2000	1927	S23 W70	S26 W70	
2	Nov 24 1997 1300	1929	N23 W65		N21 W63
3	May 17 1998 0800	1936	S25 W02	S25 W03	
4	Feb 20 1999 0600	1946	S18 W63	S21 W63	
5	Mar 11 1999 0200	1947	S18 W64	S17 W63	
6	Jun 18 1999 1500	1950	N25 W90	N24 W90	
7	Aug 7 1999 1800	1952	N22 W74		N19 W43
8	Dec 26 1999 2000	1957	N24 W31	N21 W26	
9	Mar 7 2000 1200	1960	S15 W68		S15 W69
10	May 1 2000 1100	1962	N21 W50	N20 W54	N20 W49
11	Jun 4 2000 0900	1963	S10 W62		S07 W61
12	Aug 12 2000 1400	1966	N05 W48	N13 W50	
13	Aug 22 2000 0300	1966	N30 W75	N24 W58	
14	Sep 27 2000 0800	1967	N17 W56	N18 W56	
15	Dec 22 2000 0800	1971	S12 E18	S12 E19	
16	Dec 28 2000 0100	1971	N13 W36		N12 W37
17	Apr 14 2001 1800	1975	S18 W71	S21 W62	
18	Sep 22 2001 1000	1981	S09 W65	S09 W65	
19	Apr 14 2002 1400	1988	N20 W66	N19 W57	
20	Dec 12 2002 1500	1997	N16 W36		N14 W35

Nitta selected a total of 117 impulsive SEP events between December 1994 and December 2002 by investigating data from the Low-Energy Matrix Telescope (LEMT), which is a part of the Energetic Particles: Acceleration, Composition, and Transport (EPACT) experiment on board the NASA WIND spacecraft located in a sunward, double-lunar swingby orbit. The selection criteria was based on the ^{3}He/^{4}He and Fe/O ratios in the 2-3 MeV amu^{-1} range. These events were then classified into different

categories depending on the magnitude of the above ratios. Category 1 if ^{3}He/^{4}He $>$ 0.5 and Fe and O were unobserved, category 2 if Fe/O > 0.5 and ^{3}He/^{4}He < 0.5, and category 3 if ^{3}He/^{4}He > 0.5 and Fe/O > 0.5. In order to provide source locations for these events on the surface of the sun, Nitta made use of the correlation of type III radio bursts with impulsive events. Nitta examined data from 5 hours previous to the event start time in the Radio and Plasma Wave Experiment (WAVES) on board the WIND spacecraft to determine when type III radio bursts occurred. As multiple type III bursts were likely during the SEP event time, Nitta used the occurrence of an electron-rich event to help determine which burst was likely associated with an impulsive event. This was done by looking at >30 keV electrons in WIND data to distinguish which bursts were more probable in accelerating impulsive particles. Once the event was classified, Nitta examined brightenings in the Extreme ultraviolet Imagining Telescope (EIT) on the Solar and Heliospheric Observatory (SOHO) and Soft X-ray Telescope (SXT) imagery closest to the type III burst time to determine the exact solar flare location accelerating the particles on the surface of the sun [*Nitta et al.*, 2006].

Wang selected a total of 25 impulsive events from ^{3}He rich events that occurred between 1997-2003. The selection criteria included events studied by [*Mason et al.*, 2000] and [*Mason et al.*, 2002]. ^{3}He/^{4}He and Fe/O ratios were measured by the Ultra Low Energy Isotope Spectrometer (ULEIS) instrument on board the Advanced Composition Explorer (ACE) spacecraft in the .5 MeV nucleon^{-1} range. The source region of any given event was considered to be reasonably well determined if an Hα or EIT flare was observed within a few hours of the estimated particle ejection time. The Hα information was obtained from Solar-Geophysical Data. In addition, Wang required the solar acceleration event to occur in the longitude range of $\approx W20$ to $\approx W90$, as this longitude range corresponds to the likely magnetic connection region

of the Parker spiral [*Wang et al.*, 2006].

3.3 SEP Event Discrepancies

Having compiled a list of the twenty SEP events to be used as tracers in this study, a few discrepancies arose when ensuring that these events showed impulsive characteristics. The first discrepancy came from the time of flight analysis of these particle events. The other discrepancy dealt with the variation in the author identified source region. These discrepancies are discussed in more detail in the following sections.

3.3.1 Time of Flight Analysis.

When examining the time of flight for some of these events a potential problem was encountered. The time of flight was found by determining the amount of time elapsed from the solar event eruption, as listed by the authors, and the time of SEP onset time at Earth (table 3). For example, event 2 has a time of flight of twelve minutes, in comparison light only takes eight minutes and twenty seconds to reach Earth. In order for these particles to traverse 1 AU assuming a straight radial path, they would need to travel at a velocity of $2.07 * 10^8\, m\, s^{-1}$, or nearly the speed of light, and require an acceleration to an enormous amount of energy. The three authors examined data in the 2-4 MeV range to classify these events as impulsive. Particles of this energy range take $\approx$ 2.5 hours to reach Earth; therefore, such a short travel time of twelve minutes for this event points to a misidentified SEP event. However, this event was not the only one whose time of flight was questionable.

Table 3. Time of Particle Travel (ToF) to Reach Earth from Eruption Time on Sun Given by Different Authors

SEP Number	Author	ToF[1] (hrs)	SEP Number	Author	ToF[1] (hrs)	SEP Number	Author	ToF[1] (hrs)
	Nitta	2.52		Nitta	0.20		Nitta	3.27
1	Yashiro	2.53	2^{α}	Yashiro		3	Yashiro	3.27
	Wang			Wang	0.12		Wang	
	Nitta	2.00		Nitta	1.93		Nitta	3.52
4	Yashiro	2.00	5	Yashiro	1.93	6	Yashiro	3.53
	Wang			Wang			Wang	
	Nitta	0.93		Nitta	3.82		Nitta	5.22
7	Yashiro		8	Yashiro	3.73	9^{α}	Yashiro	
	Wang	0.53		Wang			Wang	0.08
	Nitta	0.65		Nitta	1.97		Nitta	1.50
10	Yashiro	0.60	11	Yashiro		12	Yashiro	1.33
	Wang	0.60		Wang	1.78		Wang	
	Nitta	2.88		Nitta	6.75		Nitta	1.90
13	Yashiro	2.73	14^{α}	Yashiro	4.80	15	Yashiro	1.87
	Wang			Wang			Wang	
	Nitta	1.33		Nitta	0.83		Nitta	4.30
16	Yashiro	1.33	17	Yashiro	0.75	18^{α}	Yashiro	4.27
	Wang			Wang			Wang	
	Nitta	6.53		Nitta	2.42			
19^{α}	Yashiro	6.50	20	Yashiro				
	Wang			Wang	2.20			

1 Time of flight

α Time of particle arrival from eruption questionable

Events whose time of flight lay outside of the range of .5 to four hours were examined. The reasoning, behind choosing this range of times, lies in the energy range of the particles associated with these times. For a 10 MeV energetic particle, a typical travel time is around one hour. Therefore, a lower bound was set at half an hour to account for higher energy particles. For a 2 MeV particle, the travel time is around 2.5 hours and an upper bound was set at four hours to allow for lower energy particles. All events that fell outside of this range are marked in table 3. A total of five events were found to be outside this window and therefore were removed from the list of SEP tracer events as the time of arrival of these particles was unrealistic.

3.3.2 Author Identified Source Regions.

Three different authors provided the source locations of the SEP events used in this study. A requirement that at least two separate authors agree to the SEP event was imposed to lessen the chance of incorrectly identifying an impulsive event. Although each event in this study has been studied by at least two of these authors, this does not necessarily indicate the authors agree on the particular source region the event originated from (figure 8). Therefore, the models performance was dependent on whose source location was chosen as the ground truth with which to compare the models. In order to simplify the analysis and to compare the results from the model traces, Nitta was chosen as the ground truth. This was done as Nitta identified the source acceleration region of all fifteen events. This reduced any bias between the selections of the acceleration regions between the authors and allowed a single answer to be obtained. Nevertheless, with multiple identified source regions for each SEP event, there was no way for the model to give good results, if the wrong source location was initially chosen. This fact can lead to an offset of these model traces depending on which author's ground truth was used to compare to the model results.

3.4 Model Runs

With the selection of the tracer events accomplished, the next step entailed running the various models to determine magnetic connection to the sun. A total of two different linked models, as well as the Parker spiral model, were run on each event to determine this magnetic trace.

3.4.1 Parker Spiral Model.

Of all the IMF models used in this study, this model was the least mathematically intensive and requires very little input. This model assumes that the magnetic field

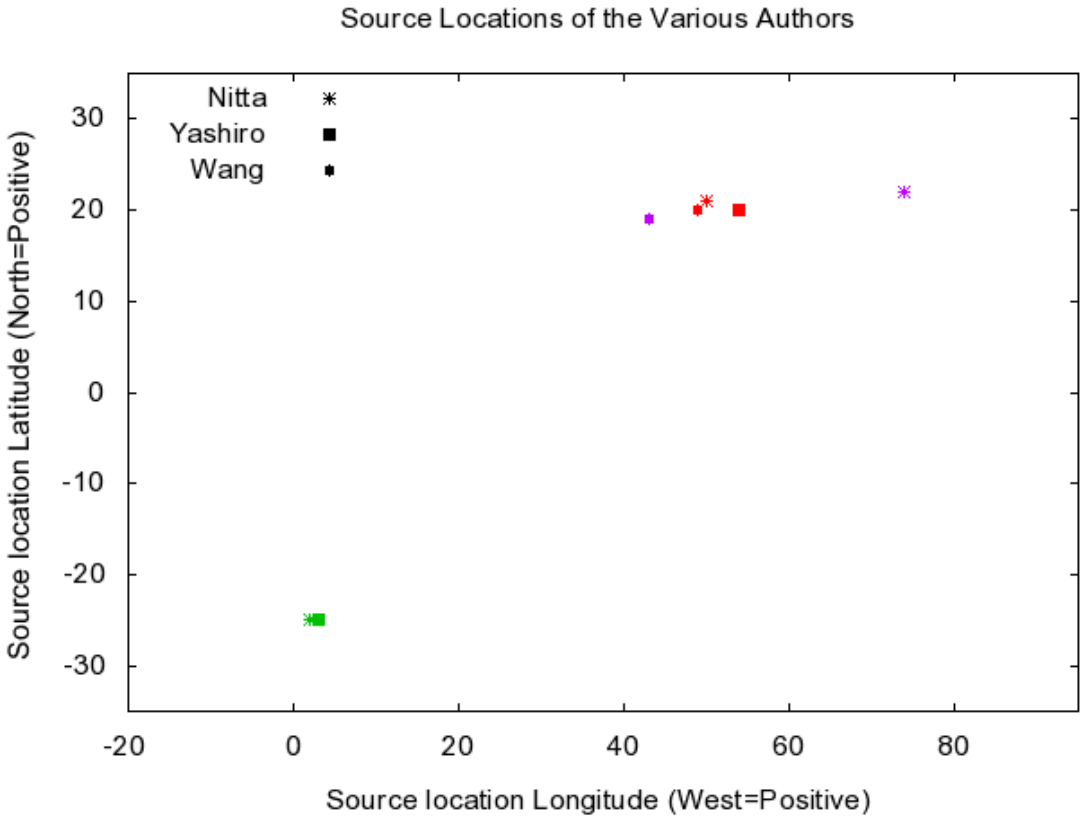

Figure 8. Author Identified Source Acceleration Regions for Three Separate Events Showing the Variation in Source Region Identification

lines that connect the sun to earth are stretched into an Archimedean spiral. With this in mind, it becomes necessary to know the solar wind speed as this was the only parameter through which the model would be affected. The solar wind speeds were taken from hourly averaged data from the Solar Wind Electron Proton Alpha Monitor (SWEPAM) instrument on board the ACE spacecraft. Out of the fifteen events selected for this study, one of these events occurred before data from the ACE spacecraft was made available. For this event, in September of 1997, it was necessary to obtain the solar wind speeds from the Solar Wind Experiment (SWE) instrument on board NASA's Global Geospace Science WIND satellite. The correlation between solar wind speeds of these two satellites (over the period of time for this study) is approximately .966. Therefore the solar wind speeds taken from the September 1997 event can be used with confidence.

The equation for the Parker model was defined in chapter II and is listed here again for reference

$$\phi_E = \Omega_{Carr}(\frac{r_E - R_{ss}}{v_{sw}}) + \phi_{CM}.$$

Having obtained the data for the solar wind speeds, it was then necessary to determine the heliographic longitude and latitude of the sun during the particular event in question. This data was downloaded using an online solar rotation applet [*Giesen*, 2009]. Collecting these two pieces of information was all that was necessary for this equation. For a tracing to the surface of the sun, the R_{ss} value in the numerator of the above equation was set to $1R_{\odot}$.

It is important to re-emphasize a few of the assumptions made when computing this model. The solar wind speed measured at 1 AU was assumed to be constant from the time the plasma left the source region on the sun. In reality, the solar wind accelerates as it moves radially outward to a point where the flow becomes supersonic. This assumption would act to shift the traced field line farther to the

west than what would have originally been predicted. Due to the mechanics of this model, only longitudes were able to be traced back to the surface of the sun, as the Archimedean spiral only affects the magnetic field lines longitude connection to the Earth.

3.4.2 PFSS and Parker Model Connection.

The PFSS model has a limited domain through which it can propagate particles. The inner boundary was set at 1 $R_{\odot}$ while the outer boundary of this model was set at $2.5R_{\odot}$. At this boundary, it becomes necessary to propagate these particles, into the IMF, out to 1 AU. To accomplish this task, the PFSS model was linked to the simple Parker spiral described above to complete the trace.

The Parker model was again run on all these events with the same assumptions above, except the R_{ss} value in the numerator of the equation was now set as the outer boundary of the PFSS model of $2.5R_{\odot}$. Tracing the magnetic field lines to the outer boundary of the PFSS model using the Parker model gives a set of coordinates which can then be fed into the PFSS model to determine their connection back to the surface of the sun. However, the Parker model only traces the longitude and provides no insight into the latitude of the field lines. In order to incorporate the latitude coordinates into the PFSS model, the location of Earth, with respect to the solar equatorial plane, was used, which was also obtained from the solar rotation applet [*Giesen*, 2009].

Once the source locations on the outer boundary of the PFSS model were determined, the focus shifts to the PFSS model. This model was run from the CCMC's online run request service. The input to this model involves the observed photospheric fields during the time of the event. These observed fields come from the synoptic magnetograms taken from several solar observatories around the world. This

model calculates magnetic fields of the solar corona assuming no currents within the region. At the outer boundary of this model, the magnetic fields are assumed to be radial where they are linked, in this case, to the Archimedean spiral of the Parker model. The magnetograms, taken as input for this model, come from the magnetic observations over the entire Carrington rotation in question.

In order to determine the magnetic connection for a specified time (i.e. to trace a particular magnetic field line), it was necessary to use the visualization software publicly available from the CCMC website. This software allows the user to input coordinates at the outer $2.5R_{\odot}$ surface and trace those field lines back to their source region on the surface of the sun. The text file output from this trace gives the coordinates where those particular field lines connect to the surface of the sun, which were then compared to the identified source region provided by Nitta.

3.4.3 WSA and ENLIL Model Connection.

The linkage, of these two models, incorporates a more complex set of physics equations than the models discussed thus far. Much like the PFSS model from the last section, the WSA model's input was obtained from magnetic observations taken from two solar observatories, the National Solar Observatory (NSO), located in Kitt Peak, AZ, and the Mount Wilson Solar Observatory (MWO), located atop Mount Wilson in Los Angeles county, California. All model traces were run from NSO data to reduce any bias from using multiple sources.

With the input data selected, the WSA could then be linked to the ENLIL model. At the $21.5R_{\odot}$ interface boundary, the WSA provided the ENLIL model with the necessary input parameters to include plasma mass, momentum and energy density. The ENLIL model then propagates these parameters through the IMF out to a distance of 1 AU.

Up to this point, the WSA-ENLIL model connection has not taken into account the specific time of the events in question. Instead, the model has run over the entire Carrington rotation period and calculated the plasma parameters over this entire range. When both models completed their runs of the Carrington rotation, it was then necessary to trace back a particular field line through the IMF. A graphics program within the WSA model was designed to pull data from the ENLIL model run and link it to the WSA run. This field line could then be traced down to the surface of the sun where the magnetic footpoint of Earth could then be identified. The exact coordinates of this Earth connected footpoint were pulled from a text file that listed the location of the magnetic footpoints for each day of the Carrington rotation plus the addition of the specific field line that was connected to Earth during the time of the SEP event.

3.5 Model Metrics and Evaluation Criteria

Having completed a model trace of these events, the next step was to determine how well the models performed based on the author identified source regions listed in table 2. To this end, an error value was assessed for the longitude and latitude field line traces using the following equations:

$$\Delta\phi = \phi_{source} - \phi_{trace} \tag{4}$$

$$\Delta\theta = \theta_{source} - \theta_{trace}. \tag{5}$$

Where ϕ_{trace} was the longitude of the traced location from the model and θ_{trace} was the traced latitude from the model. Similarly, ϕ_{source} and θ_{source} are the author identified longitude and latitude of the solar source region.

In order to determine the overall performance of the models, a Root Mean Square

(RMS) statistic was used for both the longitude and latitude offsets for each model. The RMS (equation 6) was chosen, as this statistic can take into account the variation of both positive and negative numbers. The x values in this equation represent the longitude/latitude offset values obtained when tracing with a particular model. The value of n was 15 in this case, as this was the total number of SEP events traced. In this fashion, the RMS values can be compared to each other for the different models to determine which model provided a more accurate overall trace of both the longitude and latitude.

$$RMS = \sqrt{\frac{x_1^2 + x_2^2 + ... + x_n^2}{n}} \tag{6}$$

IV. Analysis

4.1 Chapter Overview

The following sections of this chapter analyze each of the models performance on tracing the impulsive SEP events selected in chapter III. In the first section, an analysis of the various models was performed. This section was divided into three subsections each detailing a different model's analysis. The second section performed a comparison of the model's traces based on latitude and longitude. The analysis here included the physical process behind the results, comparisons to other models, and additional physical manifestations added when incorporating these models. The last section includes corrections applied to the models and their effects.

4.2 Model Performance

In the following sections the model traces are analyzed. The analysis of each model is broken into two parts; the first analyzes the longitude trace of the model, while the second part analyzes the latitude offset. Trends are identified and general comments are provided for each model.

4.2.1 Parker Model Analysis.

The Parker model derives its spiral shape of the IMF by referencing the solar wind speed of the plasma with which the magnetic field lines are considered frozen-in. By using an average solar wind speed, this would imply a likely longitude for source locations of impulsive events to originate. This preferred location can be seen in figure 9 which plots the longitude offset values versus the heliographic longitude of the identified flare site. Using a typical averaged solar wind speed of $\approx 450\,km\,s^{-1}$ as input to the Parker model results in a traced footpoint location of $\approx$ W50.

In order to calculate this longitude offset, a value of zero was assigned at the east limb (E90), a value of 180 at the west limb (W90) with 90 representing the meridian of the sun. Thus negative values of $\Delta\phi$ indicate a models traced footpoint lies farther west than the identified source region while positive values indicate a footpoint was to the east. The longitude of the flare site, depicted along the x axis in this graph, does not follow the same convention in order to facilitate the distinction of separate hemispheres on the solar surface. A negative value on this axis indicates a region on the east side of the sun, while positive values correspond to regions on the western hemisphere. The value of 0 along the x axis indicates the solar meridian. The dashed line indicates a longitude offset of zero; therefore, the closer these traces are to this dashed line, the better the model performed.

Figure 9 shows an interesting trend. The delta longitude values closest to the dashed zero line occurs very near the Parker preferred connection region (Parker sweet spot) of approximately W50. As the longitude increases, the offset values generally increase towards more positive values indicating that the models traced longitude was further to the east than the location provided by Nitta. For one event, (SEP event 6), the identified source region was located on the western limb of the sun. In order for field lines originating from this region to reach Earth under the Parker model, an associated solar wind speed of $\approx 250\,km\,s^{-1}$ would be necessary. For SEP event 6, the associated solar wind speed observed by the ACE spacecraft near Earth was $375\,km\,s^{-1}$, thus connecting the Parker model to a longitude location of W61. Such a slow solar wind speed of $250\,km\,s^{-1}$ has been observed; therefore, it is not impossible for the source region to reside near the western limb of the sun.

As the longitude decreases from the Parker sweet spot, the delta longitude values become more negative, indicating that the model traced to a location farther to the west than the identified source region. Therefore, a model bias is noticed, if the

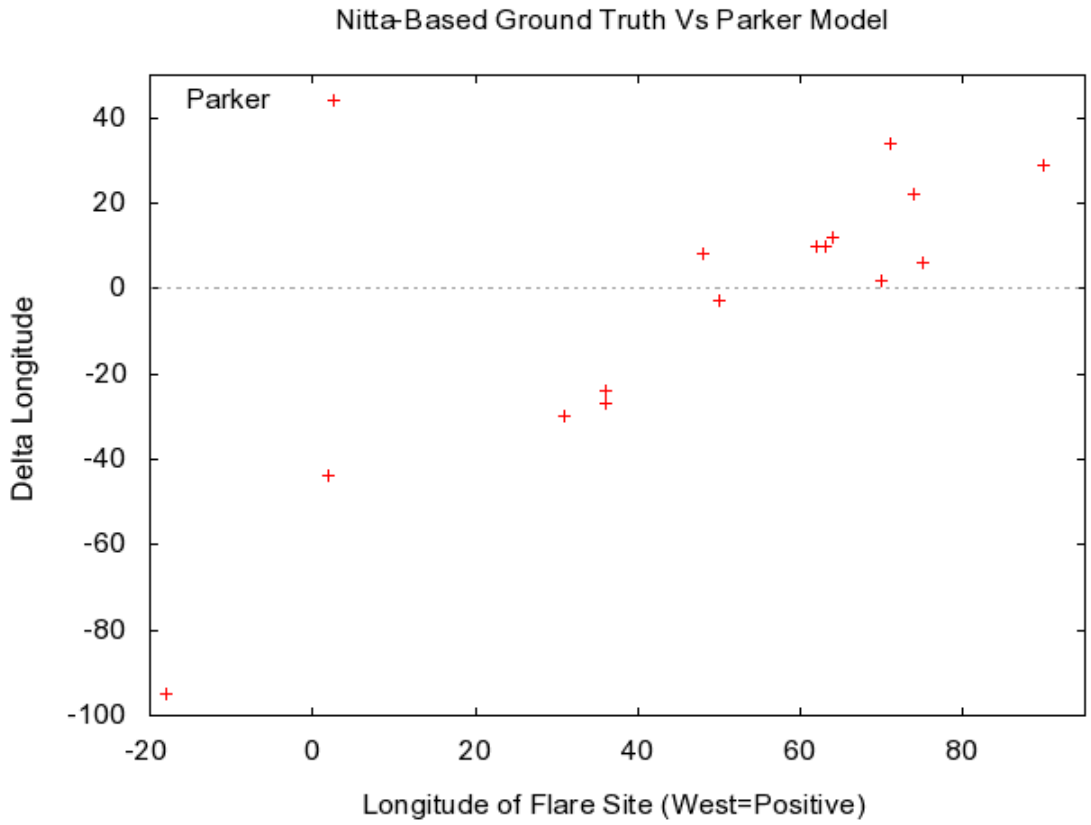

Figure 9. Longitude Offset of the Parker Spiral Model. The Dashed Line Indicates Zero Offset from Source Location

identified source region was located near the Parker sweet spot the model did a fairly good job tracing the event. However, as the source location moved farther away from this location, the offset values became larger. The rate at which these offset values became larger was higher with locations to the east of the sweet spot than with locations farther to the west.

A fundamental characteristic of the Parker spiral model was its inability to magnetically connect to the east side of the sun, regardless the speed of the solar wind. Charged particles spin along magnetic field lines and thus are usually only associated with one field line. As magnetic field lines are dragged into the IMF by the radial plasma flow of the solar wind, it becomes harder for these particles to magnetically

connect to a source region located on the eastern hemisphere. During the time of energetic particle travel to Earth, the sun has rotated a finite distance, effectively shifting the SEP source location to the west. This feature in the model raises questions with SEP event 15, as its identified source region resides on the eastern hemisphere of the sun. This fact leads to the high negative offset value expressed in SEP 15.

For events 8, 16, and 20, located near longitude W40, the corresponding solar wind speed needed for Parker connection was $\approx 600\,km\,s^{-1}$. Event 3, which had an identified source region near the meridian of the sun (W2), would require a solar wind speed of $\approx 11,000\,km\,s^{-1}$ for Parker connection. Such a solar wind speed has never been observed. In fact, the majority of solar wind measurements are below $800\,km\,s^{-1}$. This alludes to a problem in the tracing of this event using the simple Parker model, as these SEP source regions lay too close to the meridian to magnetically connect to Earth. Table 4 provides the longitude offset for each event using the Parker model.

One of the drawbacks of using this model for magnetic tracing was the models inability to allow for variations in the latitude of traced field lines. Therefore, this analysis was limited to model traced longitudes only. The longitude offsets were examined for these events and questions were raised as to the validity of certain source locations; namely those events whose source regions resided close to or on the eastern side of the sun ,as this is an unlikely connection region for the Parker model. One problem of only using the Parker model to forecast the arrival of these particles at Earth lies in the particles arriving from SEP event 15 on the eastern side of the sun. The Parker model does not connect to this location and therefore the DoD forecast would not have anticipated particles to originate from this solar source location.

Table 4. Offset Values for Parker Model Trace. Missing Sequential Number Indicate Events Removed After ToF Analysis in Chapter III

SEP Event Number	Longitude Offset	SEP Event Number	Longitude Offset
1	2	3	-44
4	10	5	12
6	29	7	22
8	-30	10	-3
11	10	12	8
13	6	15	-95
16	-24	17	34
20	-27		

4.2.2 PFSS-Parker Connection Analysis.

The PFSS-Parker model involves the connection of two separate space weather models, the inner PFSS model and an outer Parker spiral model. From chapter II, the PFSS model's domain is 1-2.5 $R_{\odot}$ and thus must be linked with the Parker model to provide a magnetic trace to Earth. Figure 10 depicts the longitude offset of this model connection using the same axis as the graphs explained in the previous section.

Figure 10 also shows an interesting trend. The longitude offset values located closest to the dashed zero line occurs near a longitude of W40, about 10 degrees east of the Parker sweet spot. Much like the Parker spiral the events that are farther west than this location are associated with positive offset values, indicating the model traced to a location farther to the east. As the longitude of the flaring region moved farther east of this W40 location, the offset values became more negative, indicating that the model traced to a location farther to the west. This again implies a bias in the model as noticed before with the Parker model. The closer the source region was to the PFSS-Parker sweet spot of W40, the better the model did, with one exception; SEP 15. This event was located on the east side of the sun and therefore the Parker model was not able to connect to this location. However, when investigating figure

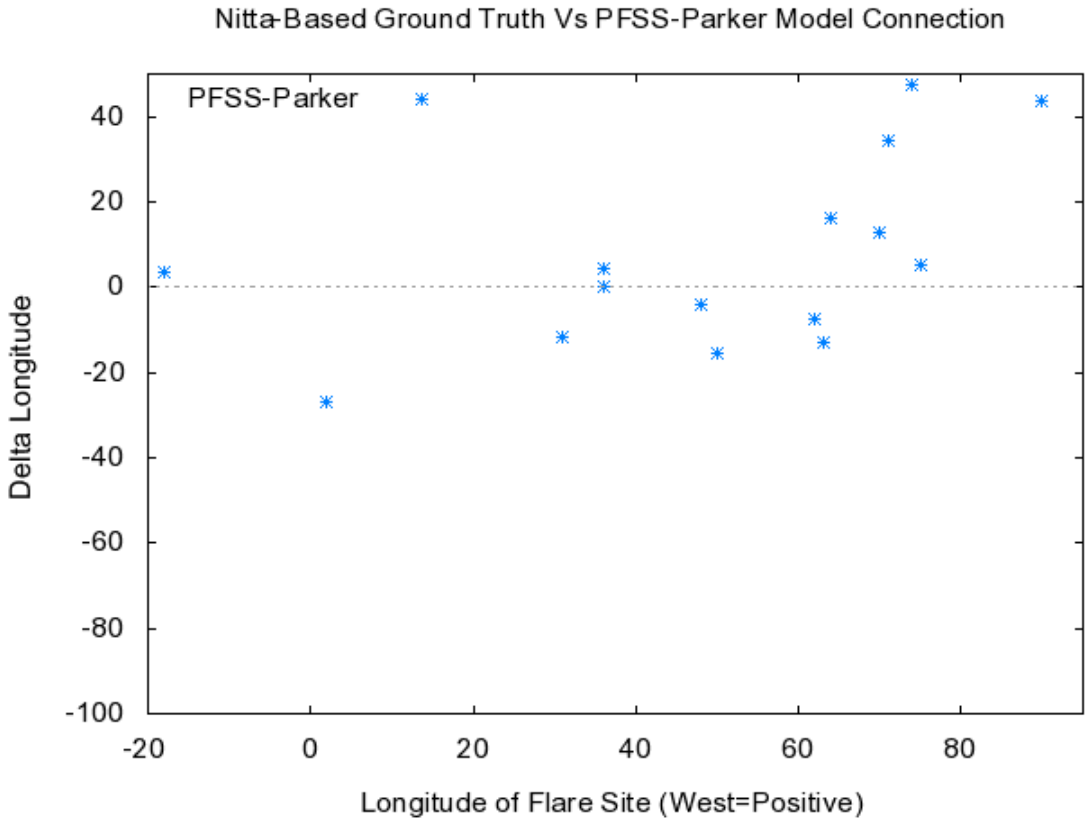

Figure 10. Longitude Offset of the PFSS-Parker Model. The Dashed Line Indicates Zero Offset from Source Location

10, this event has decreased its overall offset. Not only has the overall offset from this event decreased, the value becomes positive, indicating that the model actually traced to a location farther to the east than that identified by Nitta.

Although for this particular event, the PFSS-Parker model connection did significantly better, a general pattern cannot be deduced for more accurate tracings for events near the meridian. Investigating SEP event 3 shows a model connection farther to the west, with a longitude offset of -26.85. This indicates that the model traced to a location farther to the west. SEP Events 8, 16, and 20 have source regions near W40 and their associated longitude offsets are -11.58, 0.04,and 4.55, indicating no recognizable pattern.

This model contains the added ability to trace field line latitudes (figure 11). The PFSS model was connected directly to the Parker model, at its source surface boundary of $2.5R_{\odot}$, and the latitude coordinates for the traced field line, that were used as input to the PFSS model, were calculated using the Parker model. However, the Parker model has no ability to trace field line latitudes; instead the latitude of Earth, with respect to the equatorial plane, was used for input into the PFSS model. For this reason, it is easy to see that the PFSS model could be tracing a field line of different field line polarity than what would have been observed at Earth. Therefore, it was possible for field lines to cross the interplanetary current sheet several times when tracing through the outer IMF.

A noticeable trend in this graph was also apparent. The values that are closest to the dashed zero line occur near the equator (0 on the x axis). As the latitude of the identified source region moves farther north (positive values on x axis), the offset values become more negative, indicating that the model traced to a location that was farther to the south than what was identified by Nitta. Also, as the latitude of the source region moved farther to the south, the offset values became more positive,

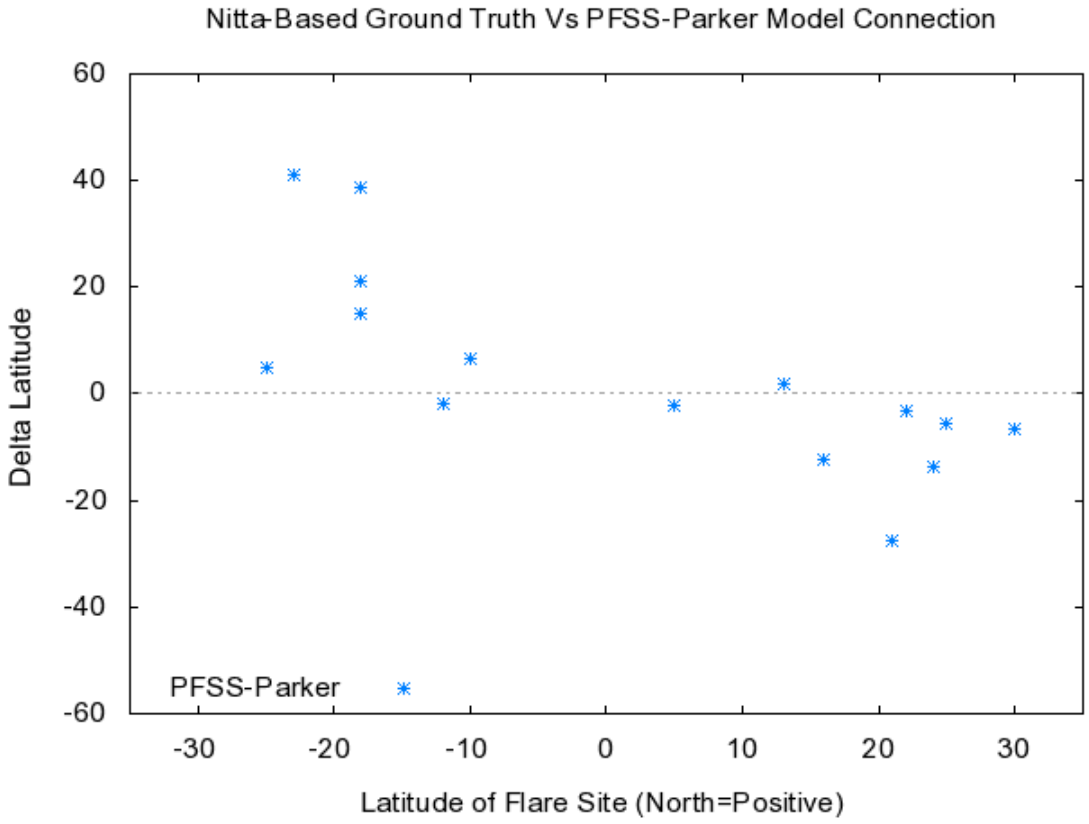

Figure 11. Latitude Offset of the PFSS-Parker Model. The Dashed Line Indicates Zero Offset from Source Location

indicating the model traced to a location that was farther to the north. Therefore, the model has a bias of performing a more accurate trace if the source location is close to the equator of the sun. This bias could arise from the input given to the PFSS model. As the Parker cannot trace the latitude of the field lines, the latitude values fed into the PFSS only varied by $\pm 7.5^{\circ}$ from the equator. These values are near the equator and one would expect the final latitude values to reside very close to the equator as well. Table 5 provides the exact longitude and latitude offset values obtained with the PFSS-Parker model connection.

Table 5. Offset Values for PFSS-Parker Model Trace. Missing Sequential Number Indicate Events Removed After ToF Analysis in Chapter III

SEP Event Number	Longitude Offset	Latitude Offset
1	12.75	41.17
3	-26.85	5.04
4	-12.83	38.69
5	16.17	15.15
6	43.75	-5.71
7	47.41	-3.05
8	-11.58	-13.74
10	-15.7	-27.41
11	-7.26	6.57
12	-4.11	-2.34
13	5.23	-6.44
15	3.64	-1.95
16	0.04	1.94
17	34.56	21.26
20	4.55	-12.35

4.2.3 WSA-ENLIL Connection Analysis.

The WSA-ENLIL is a connection of two separate models; the inner WSA model, which models the corona from the solar surface out to the outer boundary of the

current sheet component located at 21.5 $R_{\odot}$ (R_{cs}), and the outer ENLIL model that receives input from the WSA model and model the region from 21.5 $R_{\odot}$ to 1 AU. Figure 12 shows an example of the WSA output, in this case for CR 1997. This four panel plot contains important information about some solar wind parameters at R_{cs} which can later be used to assess the accuracy of this model.

The upper panel of this sample output represents the interplanetary current sheet at the R_{cs} surface. The light shade of gray indicates a positive value of B_x, magnetic field lines pointing away from the sun; whereas, the darker gray (on top of this image) indicates a negative value of B_x or magnetic field lines pointing toward the sun. The yellow line separating these two regions represents the interplanetary current sheet. The IMF was by no means static and the shape and orientation of the current sheet depicted by this output does not necessarily represent the structure of the current sheet at Earth. The scale on the left of this panel represents the latitude, where a value of zero corresponds to the equatorial plane and the values of ± 90 correspond to the solar poles. The scale on the right of the image, does not apply to this graphic as this figure only shows the direction of the fields and not the magnitude of these magnetic field lines. Along the x axis resides the Carrington longitude. Carrington longitude starts at 360° at the beginning of the rotation (the right side of these graphs) and decreases to a value of zero at rotation end. As was mentioned in chapter III, there are two observatories from which to obtain the surface magnetograms with which the WSA model was run. The observatory that provided the data for this particular model run can be found underneath the y-axis label and in this example NSO data was used. At the top of the image are dates that correspond to the progression of the Carrington rotation. In figure 12, the first date is December 1st near the beginning of the rotation (Carrington longitude near 360°) and time progresses to the left as the Carrington longitude decreases. Within the image itself, are a series of crosshairs

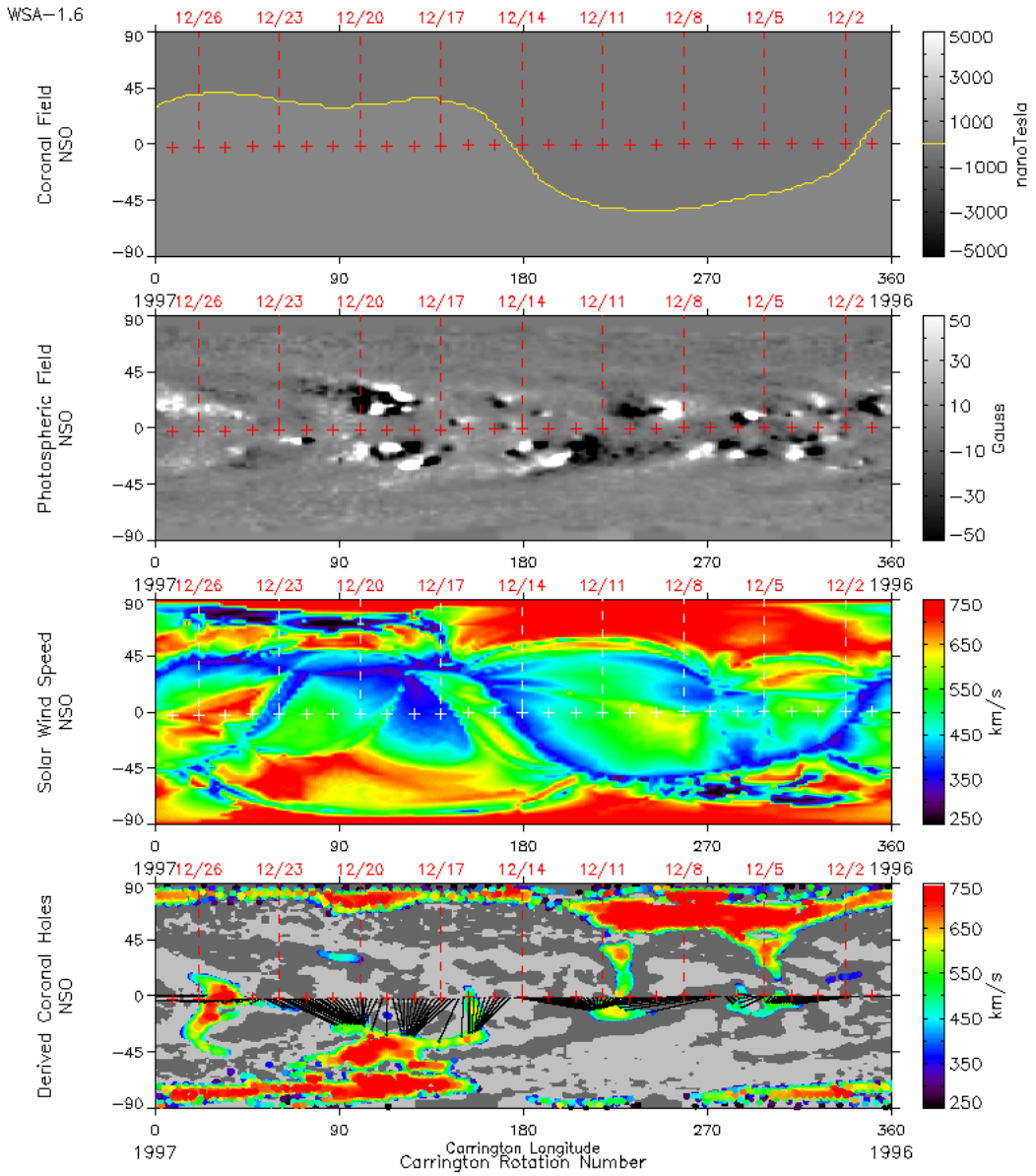

Figure 12. Sample Output for WSA Model at the R_{cs} Boundary Located at $21.5R_{\odot}$

which represent specific dates. Each crosshair indicates a new 24-hour period (synced with the start of the solar rotation) and hence spaced by $\approx 13^{\circ}$ in Carrington longitude as this was the amount of rotation the sun progresses through in one 24-hour period.

The second panel of figure 12 represents the solar surface magnetic field. As in the panel above, the light/dark gray indicates positive/negative dipolar solar magnetic field; the white and black spots at various locations represent active regions on the solar surface as seen from Earth. These images are taken directly from the corresponding observatories which can again be found underneath the y-axis label. The WSA derives its input from a synoptic magnetogram shown in the second panel of this figure. Therefore, this panel serves as an indication of the validity of the input to the WSA model.

The third panel of the figure shows a representation of the model derived solar wind at the R_{cs} surface. The scale on the right of the image indicates the speed of the flow. Note that the solar wind speeds at the poles of the sun are much higher than those near the equatorial plane. This is due to the large coronal holes near the poles of the sun where open field lines are ever present. Near the equatorial plane, the solar wind speeds are considerably less, as the closed nature of the magnetic field lines located there impedes the flow of the solar wind. This matches observations taken by the NASA Ulysses spacecraft [*Phillips et al.*, 1995] and therefore can serve as another indicator of the model's performance. This panel can be used to examine possible locations of Co-Rotating Interaction Regions (CIRs) and determine imbedded complexities within the solar wind.

The last panel of the figure is a representation of model derived coronal holes. The scale on the right of the image represents the associated solar wind speed while the gray background represents the background magnetic field of the sun. In the center of the image are a series of black lines. These indicate the models trace of magnetic field

lines that were connected to Earth throughout the course of the Carrington rotation. These lines indicate where Earth was magnetically connected at a particular time within the Carrington rotation. It was through a modified version of this graph (figure 13) that the particular region of magnetic connection for any SEP event can be determined. In this modified version, panels 2 and 4 of the previous output are expanded and the magnetic connection with Earth is depicted by the black lines. Every 24-hour window has associated with it a black line indicating its magnetic trace to Earth; therefore, there should be 27 lines across the top of the image. The particular date the field line was associated with is determined by the top of the figure. In addition to the regular 27 field lines for the Carrington rotation, this graph also includes a black line for the specific SEP event in question, allowing a specific time trace of the magnetic field to be performed. Therefore, a total of 28 lines are present along the top of this image. With the output of this model now described, an analysis of the magnetic traces can be performed.

Figure 14 shows the longitude offset values for this model trace. The events with their offsets closest to the dashed zero line occur at approximately W55. This was close to the value of the Parker sweet spot that was determined in a previous section. Much like the other models discussed thus far, the farther away from this region the events occur the higher the offset value. As the events location moves farther to the west, the offset values become more positive, indicating that the model traced to a location east of the sweet spot. As these locations move to the east, the offsets become more negative and again indicate that the model traced to a location west than the identified source region. Thus the same bias that was seen with the other models is again present in this model.

Event 3 was also studied due to the identified source region lying close to the meridian of the sun. With a negative longitude offset value of ≈ 58, the model traced

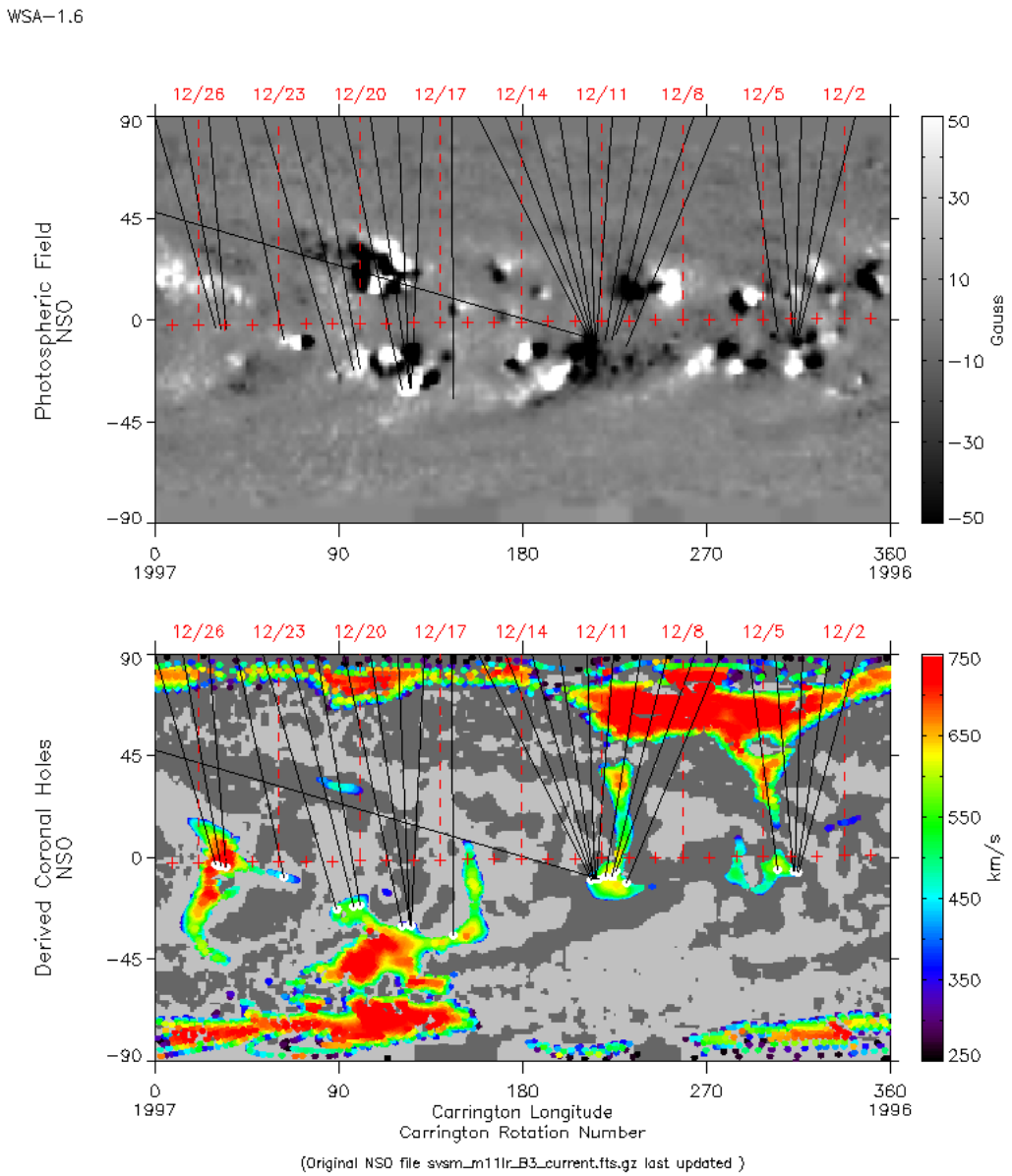

Figure 13. Modified Version of WSA Output Showing Magnetic Connection to the Sun

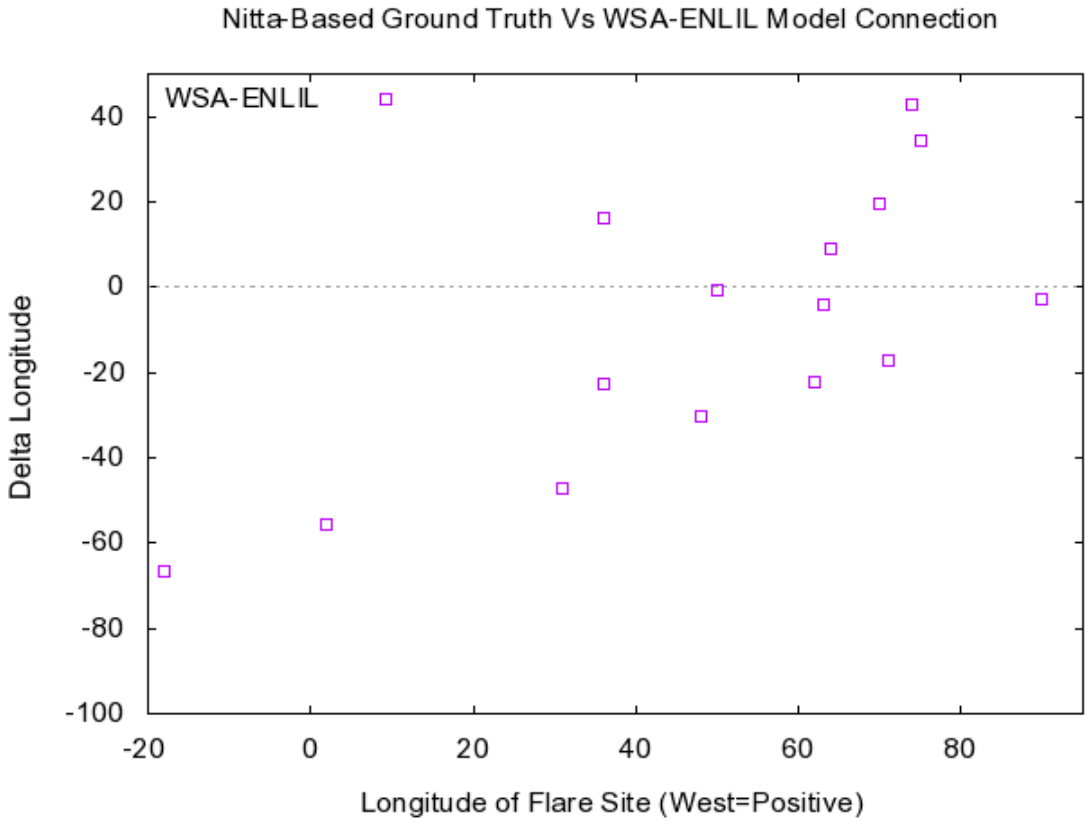

Figure 14. Longitude Offset of the WSA-ENLIL Model. The Dashed Line Indicates Zero Offset from Source Location

source region lies to the west of that identified by the authors. When comparing the longitude offsets for this event with the other model's traces, it becomes apparent that all models traced this event to a location farther to the west than its identified source region.

One of the benefits of this model linkage was the added ability to trace the latitude of the field lines from Earth to the solar surface (figure 15). Using this linked model enabled the location of the interplanetary current sheet to be traced throughout the IMF. This was the first model linkage that was able to perform this task. The simple Parker model had no ability to trace field lines and the PFSS-Parker model connection was only able to trace the field line latitudes from $2.5R_{\odot}$ to the solar surface. This graph shows similar behavior that was observed in the PFSS model. The model did a more accurate trace when the identified source region was located close to the equator of the sun and as this source region moved farther away, the offsets generally increased. Table 6 provides the exact longitude and latitude offset values obtained with the WSA-ENLIL model connection.

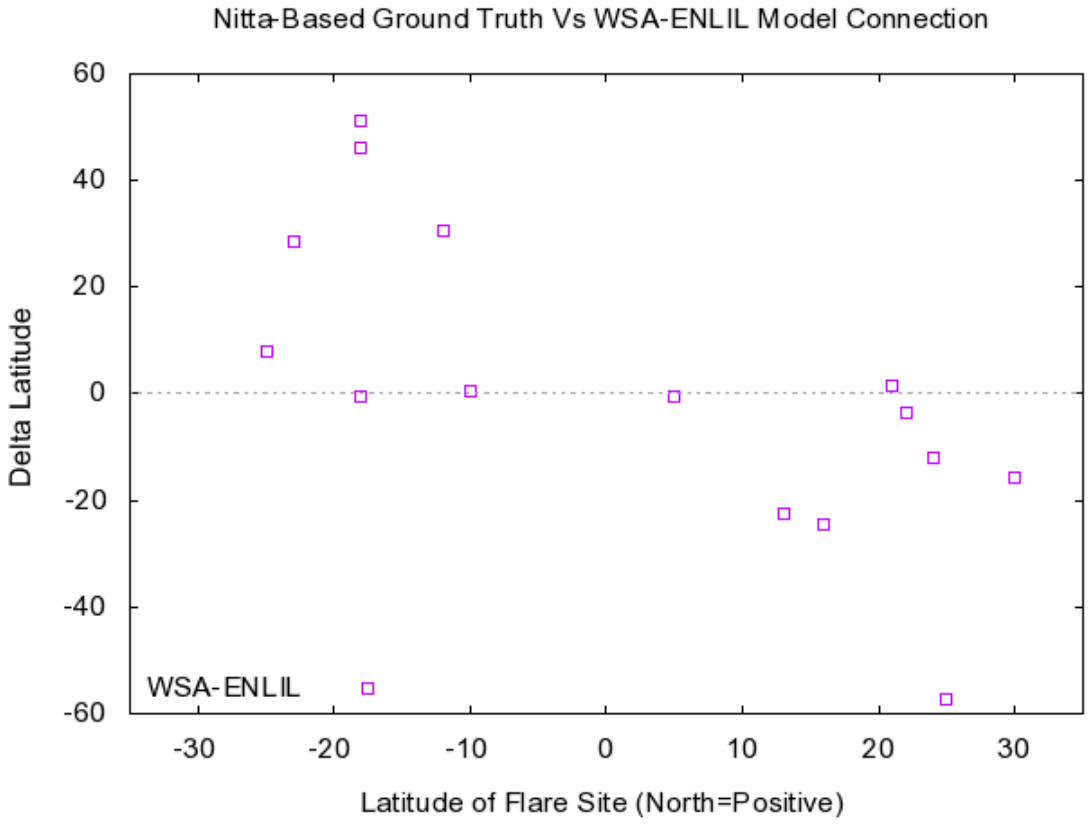

Figure 15. Latitude Offset of the WSA-ENLIL Model. The Dashed Line Indicates Zero Offset from Source Location

Table 6. Offset Values for WSA-ENLIL Model Trace. Missing Sequential Number Indicate Events Removed After ToF Analysis in Chapter III

SEP Event Number	Longitude Offset	Latitude Offset
1	19.57	28.49
3	-55.65	7.99
4	-4.07	46.26
5	8.97	-0.51
6	-2.93	-57.29
7	42.98	-3.54
8	-47.03	-11.87
10	-0.71	1.47
11	-22.34	0.53
12	-30.41	-0.60
13	34.53	-15.70
15	-66.59	30.53
16	-22.86	-22.42
17	-17.33	51.17
20	16.26	-24.54

4.3 Model Trace Comparisons

These next subsections are devoted to the comparisons of the different model traces. The first of these subsections details the comparison of the longitude traces of the models. It focuses on noticeable patterns between these traces and lists possible causes. The second subsection describes the latitude comparisons of the models capable of performing this trace.

4.3.1 Longitude Comparisons.

Figure 16 shows the longitude offsets for all fifteen events when traced using the models. The PFSS-Parker connection generally has the lowest overall offset from these events and, in general, the WSA-ENLIL connection has the largest spread over

these events. A few interesting trends are noticed when this figure is examined. As the acceleration source location moved farther to the east, the PFSS-Parker model performed a more accurate trace. However, the same cannot be said when the identified source location was moved farther to the west. At high longitudes, locations near the western limb of the sun, the PFSS-Parker model generally did not perform the most accurate trace. At these longitudes, the most accurate trace was derived from either the WSA-ENLIL model or the simple Parker model. This further points to the bias mentioned in a previous section about the PFSS-Parker model connection. Due to the sweet spot of this model connection residing farther east than that of either the WSA-ENLIL or the Parker, it should come as no surprise that these events with high longitudes will have slightly higher offset values.

Although an analysis was completed on all these events a few of these events posed some interesting findings. Throughout this analysis, attention was paid to SEP event 15 located on the eastern hemisphere of the sun. When considering the PFSS-Parker connection, the longitude offset for this event was 3.5 in comparison to the -95 value obtained with the Parker model, and the -66 value when the WSA-ENLIL model was used (figure 9). This indicates the PFSS model traced the field line to an eastern hemisphere location (E21 compared to a Parker location of W77 or W48), noted by the significant decrease in longitude offset. This trace was more accurate than the one performed by using the Parker model alone; however, a better trace does not necessarily indicate correctness. The only difference between the traces of the two models was the addition of the PFSS model to trace magnetic lines from 2.5 $R_{\odot}$ to the solar surface. From the source surface out to Earth, the same model (a Parker spiral) was used in both. While the Parker model, when traced to the solar surface, connected to a longitude region of W77, the PFSS, in a matter of only 2.5 $R_{\odot}$, shifted this field line to connect to a longitude location of E21, for a difference

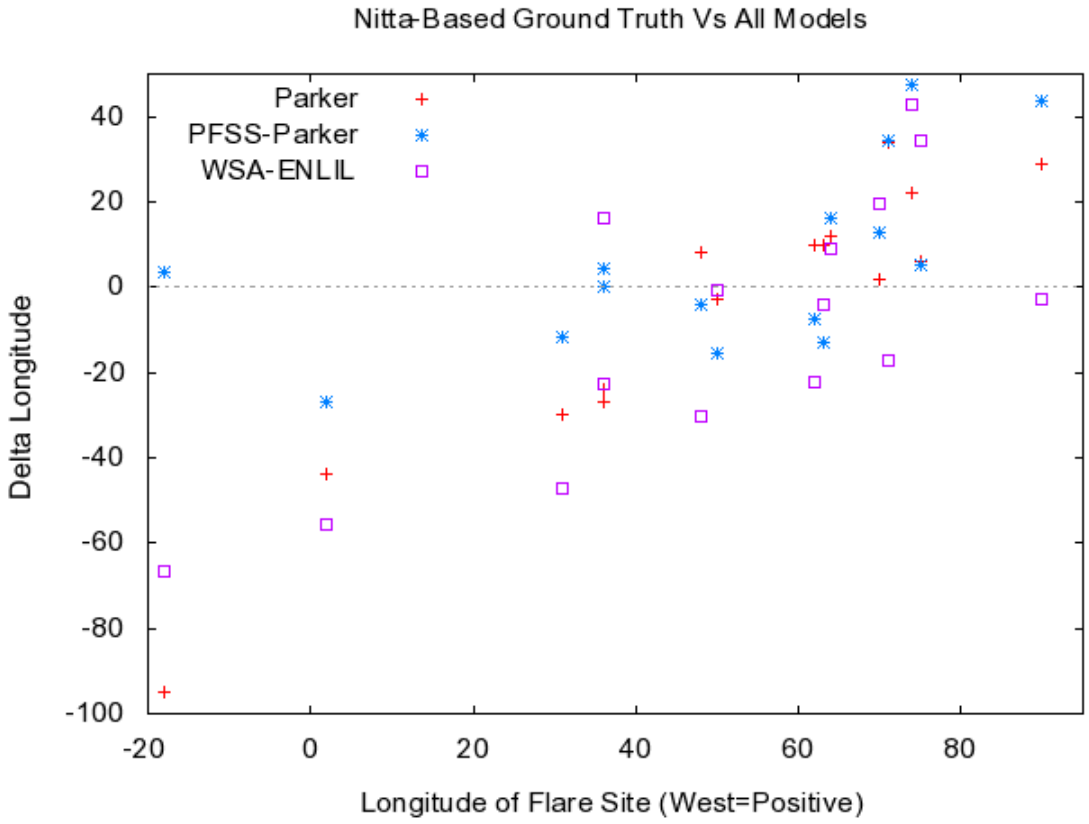

Figure 16. Longitude Offsets for all Models. The Dashed Line Indicates Zero Offset from Source Location

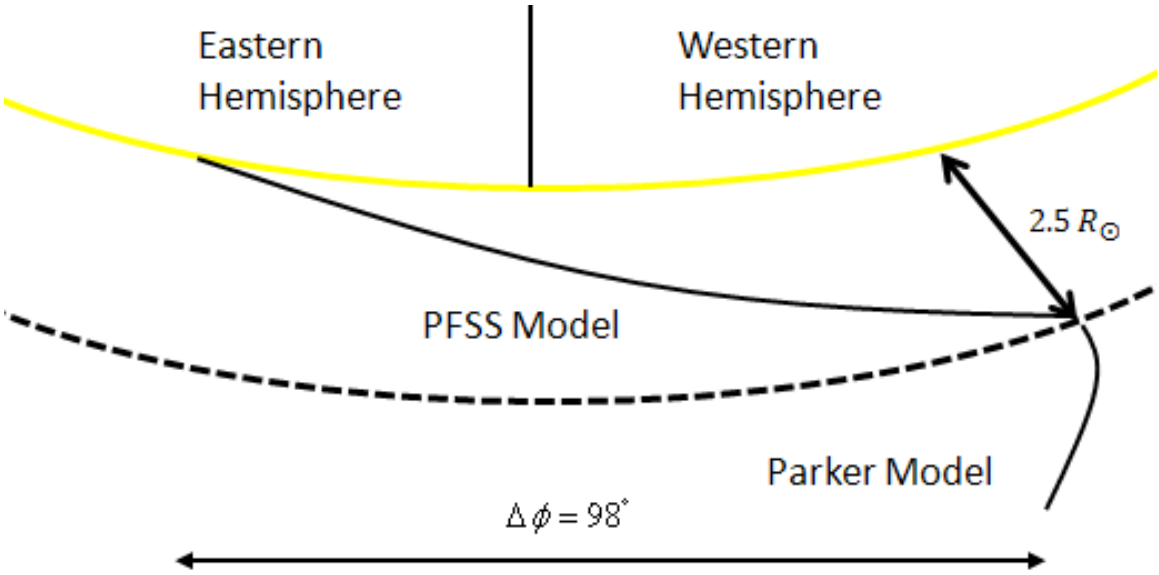

Figure 17. Longitude Trace of SEP Event 15 Using the PFSS-Parker Model Connection

of 98° in longitude (see figure 17). Although the understanding of the sun is still evolving, such a large shift in the longitude of field lines in such a short distance becomes hard to imagine. Nonetheless, without more concrete proof of the validity of the identified source location, this event was still included in the analysis.

Attention was also turned to the results obtained from tracing SEP event 3, as this events source location was questioned due to its close proximity to the meridian. Investigating figure 16 shows the PFSS model performed a more accurate trace of this event by connecting to a more easterly location than that of the Parker or WSA-ENLIL connection model. Events 8, 16, and 20 all possess identified source regions located between 25 and 40 west longitude. Comparing the longitude results from the Parker and PFSS models, show the PFSS-Parker connection model traces to a solar location farther to the east than that traced by the Parker model for the same events. The WSA-ENLIL, for the same events, displayed a higher variation in longitude offsets. Beginning with the Parker model, with longitude offsets in the range of -20 to -30 for all events, the PFSS performed a more accurate trace by decreasing

these longitude offsets to a range from 5 to -12, shifting all events eastward. The WSA-ENLIL model, on the other hand, increased the range of these offset values to a range of 20 to -45. This indicates that while the PFSS model may have had a slight tendency to trace events to a more easterly location, a similar pattern cannot be found within the WSA-ENLIL model trace. Event 8 was traced to a more westerly location while event 20 was traced to a more easterly location. Event 16 remained unchanged from the Parker models prediction, but showed a shift to the west from the PFSS model.

Event 7's source region was located on the western limb at W90. In the PFSS model's trace this event traced to a location of W46, whereas in the case of the Parker model, a longitude of W61 was found. This indicates another eastward shift in the tracing of the field lines through the PFSS model. Out of the SEP events studied so far, a trend of eastward shifts in the magnetic footpoint, when compared to those of the Parker model, has made itself apparent. Combining all PFSS longitude trace results from the 15 SEP events, it is found that 66% trace to a more easterly location than that provided by the Parker model.

One possible explanation for this shift lies in the interface boundary between the PFSS and Parker models. The PFSS treats the magnetic field lines as radial at its outer boundary. In comparison, the Parker model defines these field lines as having a spiral shape, due to the rotation of the sun in the time it takes the particles to traverse a certain distance. At the interface boundary of these two models, there exists a magnetic field line kink where the radial field lines of the PFSS merge into the spiral shape of the Parker model. This unphysical magnetic kink has the effect of causing the magnetic footpoint of the PFSS traced field line to lie farther east than the footpoint traced by the Parker model.

For the calculation of the Parker model, only the solar wind speed was needed

in order to calculate the longitude offset. The assumption made, when computing this offset, was the immediate acceleration to the speed observed at Earth. If an assumption of a typical solar wind speed of $450\,km\,s^{-1}$ was implied, it would then become possible to calculate the total offset these field lines would be shifted at the outer boundary of the PFSS model (the calculation of this offset can be found in appendix B). This value was found to be 0.59°. This small offset is not likely to account for such large shifts that are observed in a few of these events. These eastward shifts then are the likely result of a more complex tracing of the field lines by the model.

4.3.2 Latitude Comparison.

Figure 18 shows the latitude offsets for all 15 events, when traced using the models. In 53% of all SEP events, the WSA-ENLIL traced to a more southerly location than that traced by the PFSS-Parker model. The Parker model was not included in this latitude analysis as no latitude trace was available with this model. This figure shows a generally larger latitude offset for the WSA-ENLIL model connection when compared to the latitude offsets traced by the PFSS-Parker model connection. Therefore, the PFSS-Parker model performs a more accurate trace when incorporating the latitude of the magnetic field lines.

A consequence of tracing the location of the current sheet in the WSA-ENLIL model was the unlikely scattering of particles across the boundary of the current sheet throughout the inner heliosphere. Although not entirely impossible, particles that originate on one side of the current sheet are not likely to cross over to the opposite side of the current sheet.

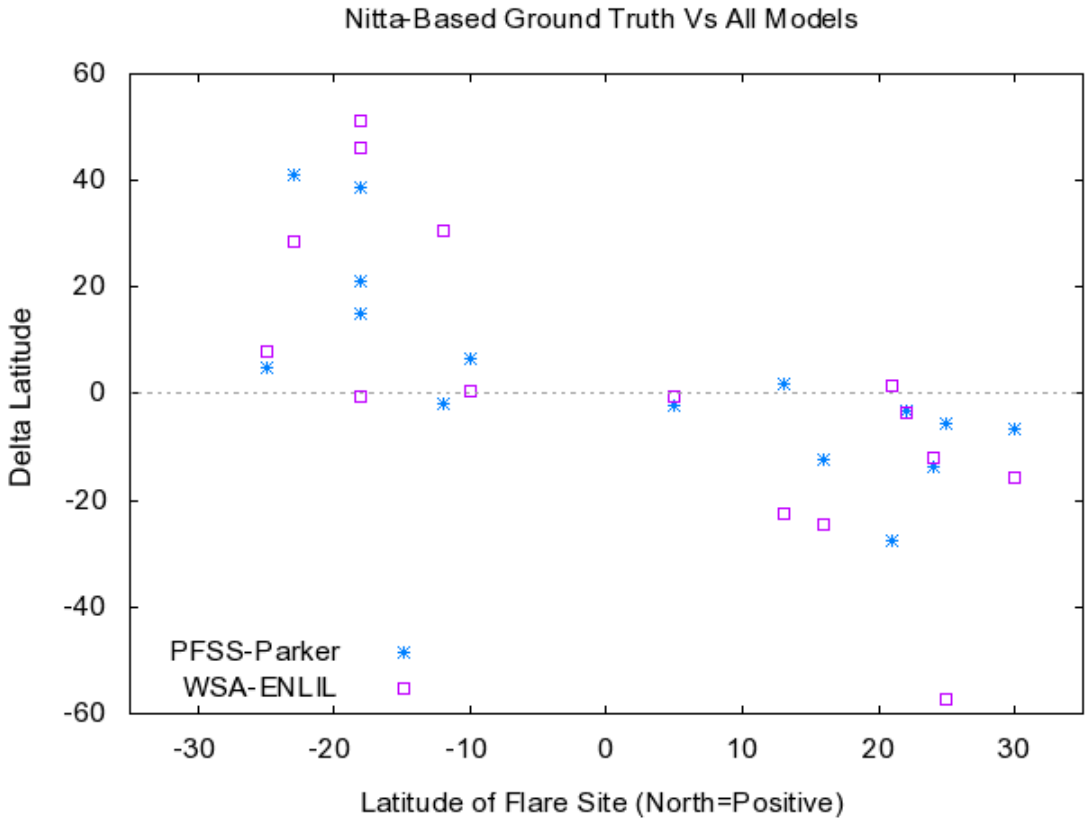

Figure 18. Latitude Offsets for all Models. The Dashed Line Indicates Zero Offset from Source Location

4.4 Model Discrepancies

Having completed an analysis of these models, corrections were suggested in order to determine if a more accurate trace could be achieved. Throughout the course of the study, many questions were raised pertaining to the validity of the tracing programs and suggestions were made in order to modify the models. These changes are described in the following sections.

4.4.1 Current Sheet Discrepancy.

As energetic particles are released from solar flares, they are scattered onto nearby open magnetic field lines. One would expect the field line, to which these particles scatter, to share the same magnetic polarity of the hemisphere from which the flare occurred, assuming that the active region was located away from the current sheet. Therefore, an energetic particle released from an impulsive source would not be expected to cross the interplanetary current sheet, and would remain on one side as it travels throughout the IMF. This analysis is constrained to the WSA-ENLIL model connection since this was the only model to track the location of the current sheet throughout the IMF. One of the benefits of this model linkage is the output from the WSA model, which represents the current sheet, among other things, at the R_{cs} surface where the ENLIL model receives its input. By examining this output it becomes possible to ensure the polarity of the magnetic field remains the same between the surface at R_{cs} and Earth.

This analysis was performed using the top panel of the WSA output (figure 12) to determine the polarity of the magnetic field line at the time of SEP event onset. This was then compared to the direction of this field at Earth from the ENLIL model output. A change in this magnetic polarity would indicate a crossing of the interplanetary current sheet by the field line within the ENLIL model's domain. The

results of this analysis are shown in table 7.

Table 7. Comparison of Magnetic Field Directions using WSA Output at Source Surface and ENLIL output at Earth

SEP Number	Polarity at $21.5R_{\odot}{}^{\alpha}$	Polarity at Earth $^{\beta}$	Models in Agreement
1	Positive$^{\eta}$	Positive	Yes
2	Negative	Negative	Yes
3	Positive	Positive	Yes
4	Positive	Negative	No
5	Positive	Positive	Yes
6	Negative	Negative	Yes
7	Positive	Negative	No
8	Negative	Negative	Yes
9	Positive	Negative	No
10	Negative	Positive	No
11	Negative	Negative	Yes
12	Negative	Negative	Yes
13	Positive	Negative	No
14	Negative	Negative	Yes
15	Negative	Negative	Yes

α Taken from Output from the WSA model
β Taken from ENLIL Model Output
η At time of particle onset, Earth was near current sheet crossing

In order to determine the polarity of the field line at the source surface, the onset time of the event was marked on the top panel of the WSA output. In some cases, the event onset times were close to a crossing of the current sheet and a simple visual analysis was not accurate enough to determine a particular side of the current sheet. There are five events in this table in which the polarity of the field lines modeled by ENLIL at Earth were different than that of the WSA output. These findings point to a problem with the magnetic field line tracing algorithm within the ENLIL model. These findings were presented to NASA's CCMC for inclusion in possible fixes for this model.

When examining the top panel of the WSA output for all SEP events, for use in determining the polarity of the magnetic field lines in the analysis above, an interesting phenomenon presented itself. Shown in figures 19 and 20 are the top panel

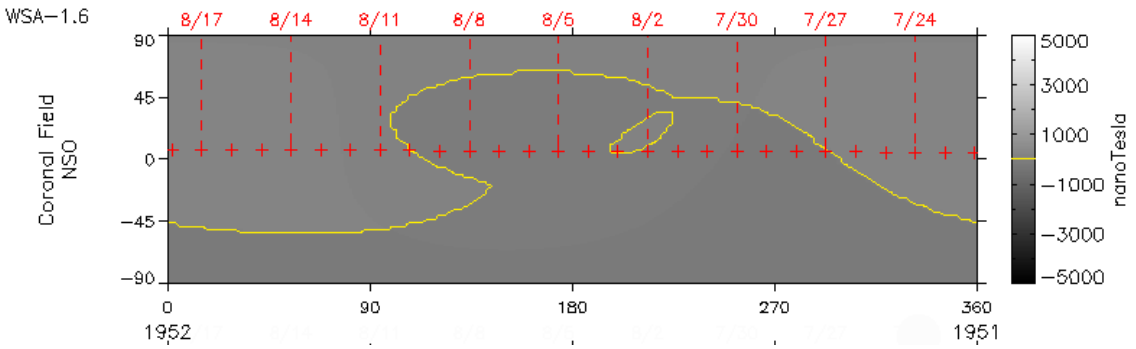

Figure 19. WSA Current Sheet Output (SEP Event 7)

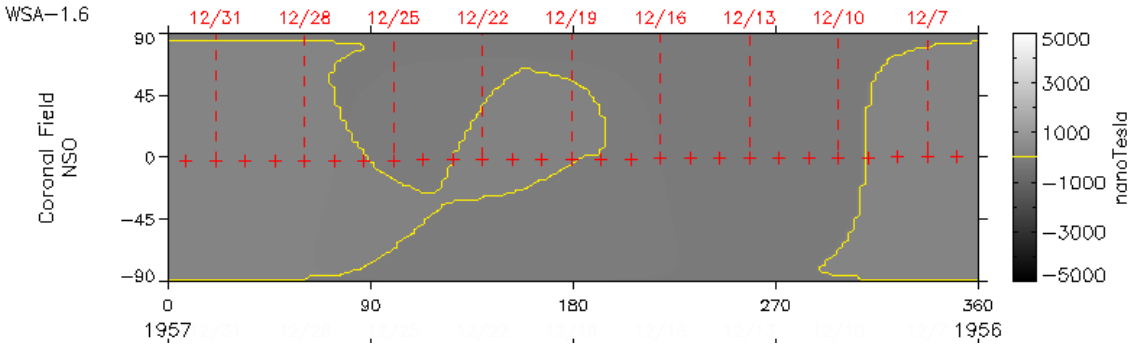

Figure 20. WSA Current Sheet Output (SEP Event 8)

WSA outputs from SEP events 7 and 8. Beginning with event 7, a hole of opposite polarity is embedded within the current sheet. This hole is completely closed off and indicates a small region of oppositely directed field lines within one side of the current sheet. When examining the next event (event 8), the current sheet seemed to have split and was no longer a horizontal feature but was rather split vertically. If this is indeed a true representation of the current sheet, this could explain the presence of opposite polarity at Earth. However, a justification of these plots is in order as this complexity raised questions on the validity of the WSA model.

Figures 21 and 22 show the top panels of the WSA output from events 6 and 10; the events preceding and just after the above mentioned events. Attention is focused on the polarity of the current sheet at the top of the image. Prior to event 6, positive B_x was on the top while negative resided on the bottom. This flip of the current sheet helped to explain the complex current sheet features noticed in events 7 and 8. The

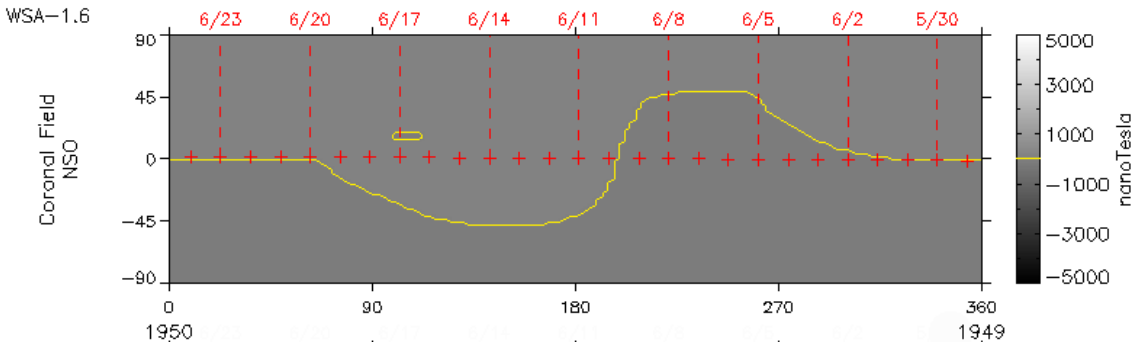

Figure 21. WSA Output before Solar Magnetic Field Reversal

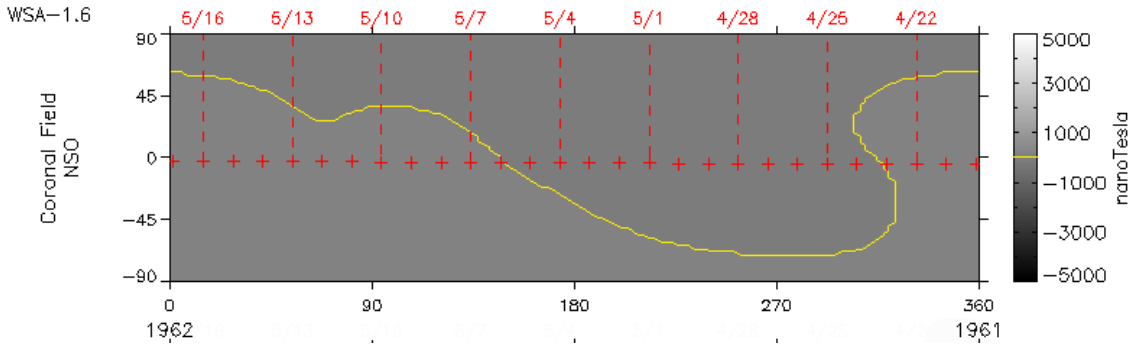

Figure 22. WSA Output after Solar Magnetic Field Reversal

reason for this flip in the current sheet could be due to the flip of the magnetic poles on the sun. All SEP events used in this study were taken from the same solar cycle (solar cycle 23). The first event occurred on November 17, 1997, while the last event (SEP 20) occurred on December 12, 2002. Over this five year period, the sun progressed approximately half way through its solar cycle and flipped its magnetic poles. Events 7 and 8 occurred in the later months of 1999 (see table 2) just before the sun peaked in its activity. According to *Babcock* [1961] the sun achieves magnetic neutralization at the time of sunspot maximum and the new reversed polarity is evidenced shortly thereafter. This could account for some of the complexities observed with these model traces.

In summary, the WSA-ENLIL model was capable of tracing magnetic field latitudes through the IMF to Earth. Particles traveling along a certain field line on one side of the current sheet are not likely to jump field lines and join a line on the oppo-

site side of the current sheet. The WSA output at R_{cs} provided insight into a problem with the tracing algorithm in the ENLIL model. Evidence of solar cycle progression is shown by the WSA model output at R_{cs} and events that occurred around this time of solar magnetic reversal are plagued with a complex current sheet structure, which makes validity of the current sheet tracing much more complicated.

4.4.2 Model Kink.

The WSA model traces magnetic field outward from the surface of the sun. One of the stipulations was that these field lines are radial at the surface and at the boundary. In addition, the WSA model does not rotate along with the sun. Therefore, in the amount of time it takes the particles to traverse to the $21.5R_{cs}$ boundary, the sun has rotated. The ENLIL model, on the other hand, has a spiral shape associated with the magnetic field lines, much like the twisted field line structure evident in the Parker spiral. It was mentioned in a previous section that there exists a non-physical kink in the field lines where the radial lines merge with the spiral lines at the boundary of the Parker and PFSS models. This kink is also evident in the WSA-ENLIL model connection (see figure 23). This kink is not only brought about by this radial field line at the boundary, but also by the non-rotation of the WSA model. Although the shift in these lines from the solar surface to the PFSS source surface located at $2.5R_{\odot}$ was determined to be negligible, the same cannot be said about the longitude offset for the WSA source surface at $21.5R_{cs}$. Assuming a constant average solar wind speed of $450\,km\,s^{-1}$, the shift in the longitude at the boundary of the WSA-ENLIL model is ≈ 5.1 (see appendix B for derivation). This offset is no longer negligible, as it could lead to a substantial change in the model trace to the solar surface. A shift was introduced to this model to account for this kink as well as the non-rotation of the WSA model solution. The results presented in this study were taken from the

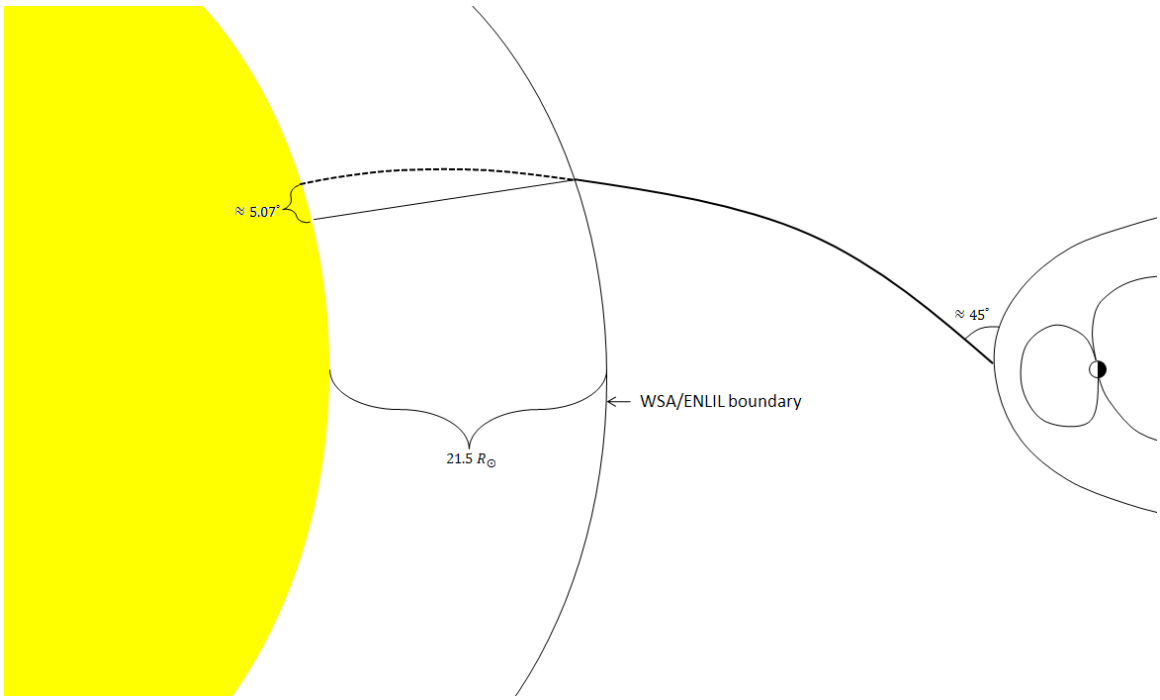

Figure 23. Magnetic Kink at Model Interface Boundary

corrected model. The correction added to this model took into account the shift at this boundary.

V. Conclusions and Future Work

5.1 Chapter Overview

This chapter is separated into two sections. The first section summarizes the analysis performed and reviews the overall performance of the linked models used in this study. The last section includes recommendations for future research.

5.2 Model Performance

Table 8 provides RMS values for the three model suites used in this study. Column three contains RMS values when considering all 15 selected impulsive SEP events for both the longitude and latitude offsets. The PFSS-Parker model connection performed the best longitude trace, followed by the Parker spiral, and lastly the WSA-ENLIL linked model. The PFSS-Parker also performed a more accurate latitude trace than did the WSA-ENLIL model connection. However, from the analysis of these events, it was found that the identified source region of SEP 15 was in question as its source region resided on the eastern side of the sun. Therefore, the fourth column of this table represents the RMS values for the SEP events with the removal of this event. Removing this event only slightly changes the longitude offset values; however, the Parker model now performed a slightly more accurate longitude trace than the PFSS-Parker connection for the longitude, while the PFSS-Parker edged out the WSA-ENLIL in the latitude traces.

Table 8. RMS Values for Model Traces versus Author Identified Source Regions with and without SEP Event 15 for Comparison

Model	Longitude/ Latitude offset	RMS Values with all events	RMS Values w/o SEP 15
Parker Spiral	Longitude	32.77	22.49
PFSS-Parker	Longitude	21.87	22.62
	Latitude	18.50	19.14
WSA-ENLIL	Longitude	32.44	28.47
	Latitude	27.51	27.29

In all, the PFSS-Parker model provides a more accurate trace in regards to both the longitude and latitude traces of the impulsive SEP events used in this study. Therefore, it is the conclusion of this study that the best suite of models for use in representing the IMF through the tracing of the impulsive SEPs was the model linkage of the PFSS with a Parker spiral. The DoD currently uses the Parker model to aid in their SEP forecasts. However, the results of this study show, in general, that the PFSS-Parker connection model provides a slightly more accurate trace ($\approx 10°$) for these impulsive SEPs. This is largely due to the fact that the PFSS-Parker models preferred location lies further to the east when compared to the Parker models sweet spot. This implies that when performing a SEP forecast, active regions that were previously classified as having a low probability for magnetic connectivity, due to the active region being located farther east than the Parker sweet spot, could, in fact, magnetically connect to Earth. If a flare were to occur during this time and accelerate the nearby plasma particles, there would be a high probability that these particles would stream along the open magnetic field lines and impact Earth. As the sun rotates by $\approx 13°$ per day, this eastward offset for the PFSS-Parker connection implies that the accelerated particles from these active region could could arrive one day earlier then would be expected by using the Parker model alone.

5.3 Future Work

Based on the findings of this study there are a few areas of future research that could provide significant value. Many of these areas focus on improving the tracing algorithms of the models in order to improve performance. These suggestions are listed in the following sections.

5.3.1 Detailed Study of SEP Event 15.

Throughout the analysis, SEP event 15 has brought about concern with its source location residing on the eastern hemisphere of the sun, as this is not a likely source region for impulsive SEPs to be accelerated from. The requirement, when selecting these events, of obtaining two separate authors who identified the event as impulsive, adds to the mystery of this event. If this region did in fact release impulsive particles then a detailed look at the PFSS model trace would be helpful. Figure 17 shows the longitude trace of this event using the PFSS-Parker model connection. The large shift in the longitude in such a short distance evidenced in the PFSS model could also be investigated.

5.3.2 Tracing of Coronal Holes.

It was the goal of this study to determine which models performed the most accurate magnetic trace of the IMF. SEP events were chosen as tracers, as these events had associated source regions which would allow a trace to be performed. Impulsive SEPs, a particular subset of SEPs, were further chosen, as these events provided a slightly more simplistic IMF. However, as this study has shown, complexities in the IMF still present a challenge when tracing it. Also, SEPs are not the perfect magnetic tracers. As was seen in this study, different authors arrived at various source acceleration regions. In addition the scattering of these particles to nearby

open field lines was assumed

Many of these complexities arise due to the active nature of the sun during these SEP events. Recall that the SEP events used in this study all occurred during the ramp up to solar maximum. If a tracing could be performed during solar minimum with little to no solar activity, it would provide confidence in the models ability to trace accurately. The problem with performing this trace is the lack of magnetic tracers during solar minimum. SEP events are accelerated from active regions on the surface of the sun, which only appear during periods of increased solar activity, making them unlikely tracers in this case. Coronal holes, on the other hand, are a solar feature present during times of solar minimum and can provide a source region to compute these traces.

The fast solar wind speed associated with coronal holes will help identify its arrival at Earth along with the presence of a co-rotating interaction region. Once the exact time of this arrival is known, a trace can be performed. A coronal hole map provided by the solar observatories would provide the source location that would be used as ground truth with which to compare these traces.

5.3.3 Complete Trace Using WSA.

Although the WSA model, at the time of this study, was not capable of performing a magnetic trace from the solar surface to Earth, valuable insight could be provided if this model were used to complete the trace. This will reduce the need to link this model with the ENLIL and may improve model performance. Performing this trace will add another model to compare the results in this study to.

Appendix A. Derivation of the Magnetic Induction Equation

The magnetic induction equation is an important equation within plasma physics that describes the relationship between plasma and magnetic field. This equation can be derived by a few simple manipulations of Maxwell's equations (listed here for reference).

Table 9. Maxwell's Equations

Ampere's Law	$\vec{\nabla} \times \vec{B} = \mu_0 \vec{J} + \mu_0 \epsilon_0 \frac{\partial \vec{E}}{\partial t}$
Gauss's Law for Magnetism	$\vec{\nabla} \cdot \vec{B} = 0$
Gauss's Law	$\vec{\nabla} \cdot \vec{E} = \frac{\rho}{\epsilon_0}$
Faraday's Equation	$\vec{\nabla} \times \vec{E} = -\frac{\partial \vec{B}}{\partial t}$

Ohm's law relates the current density $\vec{J}$ with the electric field $\vec{E}$ in space and is given by the simple equation.

$$\vec{J} = \sigma \vec{E}$$

This equation was derived off the assumption that there was no external magnetic field. This is not the case however within the Interplanetary Magnetic Field and Ohm's law must include another term to take into account the movement of the plasma within a magnetic field. This additional terms arrives from the Lorentz force equation, listed below, thus leaving a modified Ohm's law which has now taken into account the movement of the plasma within the magnetic field.

$$\vec{F} = q(\vec{E} + \vec{u} \times \vec{B}) \text{ Lorent'z Law}$$

$$\vec{J} = \sigma(\vec{E} + \vec{u} \times \vec{B}) \text{ Modified Ohm's Law}$$

If we assume that the temporal variations are slow, the displacement current ($\epsilon_0 \frac{\partial \vec{E}}{\partial t}$) is ignored in comparison with the conduction current. With this assumption the last term in Ampere's law can be eliminated leaving

$$\vec{\nabla} \times \vec{B} = \mu_0 \vec{J}$$

Substituting the modified Ohm's law equation, above, to eliminate $\vec{J}$ in Ampere's law results in the following equation

$$\vec{\nabla} \times \vec{B} = \sigma \mu_0 (\vec{E} + \vec{u} \times \vec{B})$$

Taking the curl of both sides

$$\vec{\nabla} \times (\vec{\nabla} \times \vec{B}) = \sigma \mu_0 (\vec{\nabla} \times \vec{E} + \vec{\nabla} \times (\vec{u} \times \vec{B}))$$

using the vector identity

$$\vec{\nabla} \times (\vec{\nabla} \times \vec{A}) = \vec{\nabla}(\vec{\nabla} \cdot \vec{A}) - \nabla^2 \vec{A}$$

and Faraday's law ($\vec{\nabla} \times \vec{E} = -\frac{\partial \vec{B}}{\partial t}$)gives

$$\vec{\nabla}(\vec{\nabla} \cdot \vec{B}) - \nabla^2 \vec{B} = -\mu_0 \sigma_0 \frac{\partial \vec{B}}{\partial t} + \vec{\nabla} \times (\vec{u} \times \vec{B})$$

recalling Gauss's law for magnetism ($\vec{\nabla} \cdot \vec{B} = 0$) allows the removal of the first term from the above equation. Rearranging gives the magnetic induction equation,

$$\frac{\partial \vec{B}}{\partial t} = \vec{\nabla} \times (\vec{u} \times \vec{B}) + \frac{1}{\mu_0 \epsilon_0} \nabla^2 \vec{B}.$$

The term on the left hand side is the time rate of change of the magnetic field. The first term on the right hand side, which involves the velocity of the plasma, is called the convection term while the last term, which contains the conductivity of the plasma, is called the diffusion term.

Appendix B. Math Derivations

2.1 Derivation of Field Line Offset at PFSS Parker Boundary of $2.5R_{\odot}$

$2.5R_{\odot} = 1.738 * 10^{6} km$

$v_{sw} = 450\, km\, s^{-1}$

time to reach outer boundary $\frac{1.738*10^{6} km}{450\, km\, s^{-1}} = 3863 sec$

rotation of the Sun per second is $\frac{360^{degrees}}{2.36*10^{6} sec(\text{in a carrington rotation})} = 1.53 * 10^{-4} \frac{\text{degrees}}{sec}$

total shift of the field lines at the boundary $1.53 * 10^{-4} \frac{\text{degrees}}{sec} * 3863 sec = 0.59°$

2.2 Derivation of Field Line Offset at the WSA-ENLIL Boundary of $21.5R_{\odot}$

$21.5R_{\odot} = 1.49 * 10^{7} km$

$v_{sw} = 450\, km\, s^{-1}$

time to reach outer boundary $\frac{1.49*10^{7} km}{450\, km\, s^{-1}} = 33229 sec$

rotation of the Sun per second is $\frac{360°}{2.36*10^{6} sec(\text{in a carrington rotation})} = 1.53 * 10^{-4} \frac{\text{degrees}}{sec}$

total shift of the field lines at the boundary $1.53 * 10^{-4} \frac{\text{degrees}}{sec} * 33229 sec = 5.07°$

Bibliography

Arge, C. N., and V. J. Pizzo, Improvement in the prediction of solar wind conditions using near-real time solar magnetic field updates, *jgr*, *105*, 10,465–10,480, doi:10.1029/1999JA900262, 2000.

Aschwanden, M. J., *Physics of the Solar Corona. An Introduction*, Praxis Publishing Ltd, 2004.

Babcock, H. W., The Topology of the Sun's Magnetic Field and the 22-YEAR Cycle., *Astrophysical Journal*, *133*, 572–+, doi:10.1086/147060, 1961.

Cane, H. V., R. E. McGuire, and T. T. von Rosenvinge, Two classes of solar energetic particle events associated with impulsive and long-duration soft X-ray flares, *apj*, *301*, 448–459, doi:10.1086/163913, 1986.

Cliver, E. W., and A. G. Ling, Low-Frequency Type III Bursts and Solar Energetic Particle Events, *Astrophysical Journal*, *690*, 598–609, doi:10.1088/0004-637X/690/1/598, 2009.

Cohen, C. M. S., R. A. Mewaldt, R. A. Leske, A. C. Cummings, E. C. Stone, M. E. Wiedenbeck, E. R. Christian, and T. T. von Rosenvinge, New observations of heavy-ion-rich solar particle events from ACE, *Geophysical Research Letters*, *26*, 2697–2700, doi:10.1029/1999GL900560, 1999.

Desai, M. I., G. M. Mason, R. E. Gold, S. M. Krimigis, C. M. S. Cohen, R. A. Mewaldt, J. E. Mazur, and J. R. Dwyer, Heavy-Ion Elemental Abundances in Large Solar Energetic Particle Events and Their Implications for the Seed Population, *Astrophysical Journal*, *649*, 470–489, doi:10.1086/505649, 2006.

Forbush, S. E., Three Unusual Cosmic-Ray Increases Possibly Due to Charged Particles from the Sun, *Physical Review*, *70*, 771–772, doi:10.1103/PhysRev.70.771, 1946.

Foukal, P. V., *Solar Astrophysics, 2nd, Revised Edition*, 2004.

Giesen, J., Solar rotation applet, `http://www.jgiesen.de/sunrot/index.html`, 2009.

Gopalswamy, N., Coronal Mass Ejections and Type II Radio Bursts, *Washington DC American Geophysical Union Geophysical Monograph Series*, *165*, 207–+, 2006.

Gurnett, D. A., and A. Bhattacharjee, *Introduction to Plasma Physics*, 2005.

Kahler, S. W., Origin and Properties of Solar Energetic Particles in Space, *Space Weather, ed. P. Song, H. J. Singer, and G. L. Siscone, Geophysical Monograph 125,109-122*, *125*, 109–122, 2001.

Klimchuk, J. A., Theory of Coronal Mass Ejections, *Space Weather (Geophysical Monograph 125), ed. P. Song, H. Singer, G. Siscoe (Washington: Am. Geophys. Un.), 143 (2001)*, *125*, 143–+, 2001.

Kurt, V., A. Belov, H. Mavromichalaki, and M. Gerontidou, Statistical analysis of solar proton events, *Annales Geophysicae*, *22*, 2255–2271, 2004.

Lanzerotti, L., D. Baker, T. Jernigan, D. Knipp, R. Williamson, and S. Worden, Report of the Assessment Committee for the National Space Weather Program, 2006.

Laurenza, M., E. Cliver, J. Hweitt, M. Storini, A. G. Ling, C. Balch, and M. Kaiser, A Technique for Short-Term Warning of Solar Energetic Particle Events Based on Flare Location, Flare Size, and Evidence of Particle Escape.

Mason, G. M., J. R. Dwyer, and J. E. Mazur, New Properties of ^{3}HE-rich Solar Flares Deduced from Low-Energy Particle Spectra, *The Astrophysical Journal Letters*, *545*, L157–L160, doi:10.1086/317886, 2000.

Mason, G. M., et al., Spectral Properties of He and Heavy Ions in ^{3}He-rich Solar Flares, *Astrophysical Journal*, *574*, 1039–1058, doi:10.1086/341112, 2002.

Moore, R. L., and A. C. Sterling, Initiation of Coronal Mass Ejections, *Washington DC American Geophysical Union Geophysical Monograph Series*, *165*, 43, 2006.

Nitta, N. V., D. V. Reames, M. L. DeRosa, Y. Liu, S. Yashiro, and N. Gopalswamy, Solar Sources of Impulsive Solar Energetic Particle Events and Their Magnetic Field Connection to the Earth, *Astrophysical Journal*, *650*, 438–450, doi:10.1086/507442, 2006.

Phillips, J. L., et al., Ulysses Solar Wind Plasma Observations at High Southerly Latitudes, *Science*, *268*, 1030–1033, 1995.

Prölss, G. W., *Physics of the Earth's Space Environment: an introduction*, Springer-Verlag Berlin Heidelberg, 2004.

Reames, D. V., Solar energetic particles: A paradigm shift, *Reviews of Geophysics*, *33*, 585–590, doi:10.1029/95RG00188, 1995.

Reames, D. V., and C. K. Ng, Heavy-Element Abundances in Solar Energetic Particle Events, *Astrophysical Journal*, *610*, 510–522, doi:10.1086/421518, 2004.

Reames, D. V., J. P. Meyer, and T. T. von Rosenvinge, Energetic-particle abundances in impulsive solar flare events, *Astrophys. J. Suppl. Ser.*, *90*, 649–667, doi:10.1086/191887, 1994.

Riley, P., J. A. Linker, Z. Mikić, R. Lionello, S. A. Ledvina, and J. G. Luhmann, A Comparison between Global Solar Magnetohydrodynamic and Potential Field Source Surface Model Results, *Astrophysical Journal*, *653*, 1510–1516, doi:10.1086/508565, 2006.

Schatten, K. H., J. M. Wilcox, and N. F. Ness, A model of interplanetary and coronal magnetic fields, *solphys*, *6*, 442–455, doi:10.1007/BF00146478, 1969.

Tylka, A. J., C. M. S. Cohen, W. F. Dietrich, M. A. Lee, C. G. Maclennan, R. A. Mewaldt, C. K. Ng, and D. V. Reames, Shock Geometry, Seed Populations, and the Origin of Variable Elemental Composition at High Energies in Large Gradual Solar Particle Events, *apj*, *625*, 474–495, doi:10.1086/429384, 2005a.

Tylka, A. J., C. M. S. Cohen, W. F. Dietrich, M. A. Lee, C. G. Maclennan, R. A. Mewaldt, C. K. Ng, and D. V. Reames, Shock Geometry, Seed Populations, and the Origin of Variable Elemental Composition at High Energies in Large Gradual Solar Particle Events, *apj*, *625*, 474–495, doi:10.1086/429384, 2005b.

Wang, Y.-M., M. Pick, and G. M. Mason, Coronal Holes, Jets, and the Origin of ^{3}He-rich Particle Events, *Astrophysical Journal*, *639*, 495–509, doi:10.1086/499355, 2006.

Yashiro, S., N. Gopalswamy, E. W. Cliver, D. V. Reames, M. L. Kaiser, and R. A. Howard, Association of Coronal Mass Ejections and Type II Radio Bursts with Impulsive Solar Energetic Particle Events, in *The Solar-B Mission and the Forefront of Solar Physics*, *Astronomical Society of the Pacific Conference Series*, vol. 325, edited by T. Sakurai and T. Sekii, pp. 401–+, 2004.

REPORT DOCUMENTATION PAGE

Form Approved
OMB No. 0704-0188

1. REPORT DATE *(DD-MM-YYYY)*	2. REPORT TYPE	3. DATES COVERED *(From - To)*
25-03-2010	Master's Thesis	Aug 2009 - Mar 2010

4. TITLE AND SUBTITLE
Evaluation of Interplanetary Magnetic Field Tracing Models Using Impulsive SEPs

5a. CONTRACT NUMBER

5b. GRANT NUMBER

5c. PROGRAM ELEMENT NUMBER

6. AUTHOR(S)

Elliott, Brian P., 2d Lt, USAF

5d. PROJECT NUMBER

5e. TASK NUMBER

5f. WORK UNIT NUMBER

7. PERFORMING ORGANIZATION NAME(S) AND ADDRESS(ES)
Air Force Institute of Technology
Graduate School of Engineering and Management (AFIT/EN)
2950 Hobson Way
WPAFB, OH 45433-7765

8. PERFORMING ORGANIZATION REPORT NUMBER
AFIT/GAP/ENP/10-M05

9. SPONSORING/MONITORING AGENCY NAME(S) AND ADDRESS(ES)
NASA/Community Coordinated Modeling Center
NASA/GSFC Code 674
Greenbelt, MD 20771
(301)286-2061

10. SPONSOR/MONITOR'S ACRONYM(S)
NASA/CCMC

11. SPONSOR/MONITOR'S REPORT NUMBER(S)

12. DISTRIBUTION/AVAILABILITY STATEMENT

APPROVED FOR PUBLIC RELEASE; DISTRIBUTION UNLIMITED

13. SUPPLEMENTARY NOTES

14. ABSTRACT

Current Interplanetary Magnetic Field (IMF) models are evaluated in this study to determine which model(s) perform an accurate representation of this magnetic structure. These IMF models include the Parker Spiral model, the Potential Field Source Surface (PFSS) model, the Wang-Sheeley-Arge (WSA) model and the ENLIL model. Impulsive Solar Energetic Particles (SEPs) are used as tracers to determine the magnetic structure of the IMF and provide source locations for model comparisons. Each individual model is analyzed, compared to the identified solar source region and a longitude/latitude offset of these traces assigned. The model connection of the PFSS and Parker models is found to provide the lowest latitude and longitude offsets from the identified source regions with RMS values of 21.9 and 18.5 respectfully. Model discrepancies are investigated and suggestions are made to improve model tracing performance.

15. SUBJECT TERMS

Impulsive Solar Energetic Particles, Interplanetary Magnetic Field, Magnetic Field Tracings, Space Weather Modeling, Solar Energetic Particle Forecasting

16. SECURITY CLASSIFICATION OF:			17. LIMITATION OF ABSTRACT	18. NUMBER OF PAGES	19a. NAME OF RESPONSIBLE PERSON
a. REPORT	b. ABSTRACT	c. THIS PAGE			Acebal, Ariel O., Lt Col, USAF (ENP)
U	U	U	UU	90	19b. TELEPHONE NUMBER *(Include area code)* (937)255-3636,x4518 ariel.acebal@afit.edu

Reset